Title

To Be or Not to Be an Oocyte: Msps/XMAP215 Controls Oocyte Cell Fate in the *Drosophila* Ovary

Authors

Wen Lu[1]*, Margot Lakonishok[1], Hannah Neiswender[2], Graydon B. Gonsalvez[2], Vladimir I. Gelfand[1]*

Affiliations

[1]Cell and Developmental Biology, Northwestern University, Feinberg School of Medicine, Chicago, IL 60611.

[2]Cellular Biology and Anatomy, Medical College of Georgia, Augusta University, GA 30912.

*Corresponding authors: Wen Lu (w-lu@northwestern.edu) (ORCID 0000-0002-8849-8100); Vladimir I. Gelfand (vgelfand@northwestern.edu) (ORCID 0000-0002-6361-2798)

Short title

Msps/XMAP215 promotes Oocyte Fate Determination

Abstract

Cell fate determination is fundamental to development. In the *Drosophila* ovary, a 16-cell germline cyst forms in which two pro-oocytes arise; one is selected as the oocyte, while the remaining 15 cells differentiate into nurse cells. Here, we identify Mini spindles (Msps), a *Drosophila* XMAP215-family microtubule polymerase, as a key regulator of oocyte fate specification. Msps mRNA and protein are enriched in the pro-oocytes prior to oocyte specification. Inhibition of Msps prevents oocyte specification and disrupts the accumulation of the oocyte marker Orb, producing egg chambers with 16 nurse cells. Optogenetic recruitment of Msps increases microtubule polymerization and promotes Orb accumulation in nurse cells, suggesting that Msps activity is sufficient to initiate the oocyte fate determination. Furthermore, Msps associates with the germline-specific organelles, the spectrosome and fusome, and becomes asymmetrically distributed, biasing the two pro-oocytes toward oocyte fate. We propose that an Msps–dynein feedback loop amplifies small initial differences between the two pro-oocytes to specify a single oocyte.

Teaser

A self-reinforcing cytoskeletal feedback loop selects a single egg cell from a cluster of interconnected germ cells.

MAIN TEXT

Introduction

In the *Drosophila* ovary, oocyte specification takes place within the anterior-most region of each ovariole, the germarium. The germarium is organized into several regions that support stepwise germ cell development. Germline stem cells (GSCs) are located at the anterior tip and divide asymmetrically to produce cystoblasts (CBs). Each CB undergoes four rounds of incomplete mitotic divisions, giving rise to 16 interconnected cystocytes. These cell divisions occur in region 1, while region 2a contains newly formed interconnected 16-cell cysts. As cysts progress into region 2b, they become lens-shaped and are enveloped by somatic follicle cells. In region 3, the 16-cell cyst becomes fully encapsulated by a monolayer of follicle cells and buds off as an individual egg chamber, marking the beginning of oogenesis in the vitellarium (stage 1) (Fig. 1A) (*1*).

The spectrosome is a spherical precursor of the fusome, a membranous cytoskeleton-rich organelle, and is present in GSCs and CBs, where it helps to orient asymmetric divisions (*2*). During subsequent divisions, the spectrosome transforms into the branched fusome. The fusome plays a critical role in anchoring the mitotic spindle during germ cell division, establishing cyst polarity and directing the asymmetric distribution of cell fate determinants, as well as organizing the microtubule network (*3, 4*). Although the fusome connects all 16 cystocytes through intercellular cytoplasmic bridges, known as ring canals, it is biased toward the two oldest cells, which inherit the most fusome material (*5*). This bias correlates with entry into meiosis and pro-oocyte identity, as indicated by C(3)G staining (a synaptonemal complex component)(*6*).

Notably, C(3)G can be detected in more than two cystocytes in region 2a, reflecting the well-described transient meiotic entry of additional cells. Subsequently, meiosis becomes restricted to two pro-oocytes in region 2b: one maintains meiosis and is selected as the oocyte, whereas the other pro-oocyte exits meiosis (*7*). All other cystocytes, including the non-selected pro-oocyte, then enter endoreplication and differentiate into 15 nurse cells (Fig. 1A) (*8*). Oocyte selection is marked by the enrichment of key molecular markers such as Orb, an RNA-binding protein essential for oocyte identity and axis specification (*9, 10*), as well as by the accumulation of centrosomes migrated from sister nurse cells (*11, 12*). Nurse cells then synthesize mRNAs and proteins, and deliver these materials to the developing oocyte through the ring canals to support rapid oocyte growth (*8, 13-15*).

Oocyte specification depends on several molecular complexes that act in concert. 1) The fusome: loss of essential components such as the Adducin-like gene *hu li tai shao* (*hts*) (*16*) and α-Spectrin (*17*), disrupts fusome architecture and abolishes oocyte specification, yielding cysts with only nurse cells. 2) The microtubule network: disruption of the polarized microtubule network (*18*) or lack of its key regulators, such as microtubule minus-end binding protein Patronin/CAMSAP (*7*) and the actin-microtubule crosslinker Short stop (Shot) (*13, 19, 20*), prevents oocyte specification. 3) Dynein-based transport: loss of dynein heavy chain (Dhc64C) (*21*), or its cofactors Bicaudal-D (BicD) (*22*), Egalitarian (Egl) (*23*), and Lis1 (*24*) results in cysts with 16 polyploid nurse cells and no diploid oocyte. 4) RNA-binding protein: Orb is essential for oocyte specification (*9, 25*) and promotes translational activation of key oocyte mRNAs, including *oskar* (*26*) and *gurken* (*27*), which are required for axis formation in the oocyte

(*28*). In summary, the fusome organizes a polarized microtubule network with the minus ends enriched in the future oocyte, enabling dynein-dependent transport of oocyte-specific factors to concentrate in this cell. This robust polarized transport along the microtubule network ensures the selection and maintenance of a single oocyte in each cyst. Recent work has shown that Shot and its interacting partner Patronin/CAMSAP establish an asymmetric microtubule minus-end network through their association with the fusome (*7, 20, 29*). However, the upstream factor(s) that initiate microtubule growth and organization, particularly the establishment of plus-end organization that supports directional transport to define oocyte specification, have remained unclear.

We previously demonstrated that the microtubule polymerase Mini Spindles (Msps), the *Drosophila* homolog of XMAP215, is essential for oocyte growth and fate maintenance (*30*). Furthermore, Msps/XMAP215 is required for the structure and function of cytoplasmic microtubules during oogenesis, as well as for the microtubule-dependent nurse cell-to-oocyte transport and localization of *bicoid (bcd)* mRNA, a maternal anterior determinant (*31*). Msps/XMAP215 contains an N-terminal array of five conserved TOG (tumor overexpressed gene) domains (Fig. 1B) (*32*). Msps/XMAP215 tracks the microtubule plus-ends and enhances microtubule polymerization rate by increasing tubulin dimer concentration at the growing tips (*33, 34*). TOG1–2 engage free tubulin, and TOG5 associates with lattice-incorporated tubulin, while TOG3–4 function as a bridge that stabilizes the intermediate conformation between soluble and incorporated tubulin (Fig. 1A) (*35*). Loss of Msps/XMAP215 disrupts spindle integrity, producing abnormally short or disorganized spindles during mitosis and meiosis in *Drosophila* (*36-38*). In the ovary, we showed that dynein-dependent transport

concentrates *msps* mRNA and Msps protein in the oocyte, where it stimulates microtubule polymerization and enhances nurse cell–to–oocyte transport, which is essential for oocyte growth and oocyte fate maintenance (*30*).

In this study, we show that Msps/XMAP215 is not only essential for maintaining oocyte fate but also plays a key role in oocyte specification. We find that *msps* mRNA and Msps protein are enriched in pro-oocytes before oocyte selection. Loss of Msps disrupts oocyte specification, as evidenced by the failure to accumulate key oocyte markers such as Orb and Patronin, resulting in egg chambers containing 16 nurse cells and no oocyte. Remarkably, optogenetic recruitment of Msps enhances microtubule polymerization and increases Orb level in nurse cells, suggesting that Msps activity is sufficient to promote the initial oocyte fate determination. Finally, we show that Msps associates with the spectrosome and fusome and is asymmetrically inherited by pro-oocytes, supporting a model in which localized Msps-stimulated microtubule growth provides a competitive advantage to one cell and initiates a positive feedback loop to reinforce oocyte specification.

Results

Msps is concentrated in pro-oocytes and early oocytes

A polarized microtubule network is essential for oocyte specification in the *Drosophila* germarium (*8*). We, therefore, examined the localization of the microtubule polymerase Msps in the germarium. Using single-molecule inexpensive fluorescence *in situ* hybridization (smiFISH) (Fig. 1B), we found that *msps* mRNA is enriched in discrete foci beginning in region 2a, preceding detectable accumulation of the oocyte marker Orb (Fig. 1C–1D). This suggests that *msps* mRNA enrichment marks an early step in oocyte specification, before Orb-dependent mechanisms are established.

To analyze protein distribution, we used two CRISPR knock-in lines: an indirect labeling by the NanoTag VHH05 that can be recognized by fluorescently-tagged nanobodies (*30, 39*) (Msps-3XVHH05 with NbVHH05-EGFP or NbVHH05-3XTagRFP) and a direct C-terminal EGFP fusion (Msps-EGFP) (Fig. 1B). Both alleles are homozygous viable and fertile, indicating that the tags do not impair protein function. In both cases, Msps protein was enriched in pro-oocytes from region 2a and became progressively concentrated in the oocyte in regions 2b and 3 (Fig. 1E–1F′; movie S1). In regions 2a and 2b, we identified the two pro-oocytes as the central cystocytes with four ring canals, using GFP-Pavarotti (kinesin-6) to label ring canals together with Hts (1B1) staining of the fusome. We observed that Msps recognized by a fluorescently-tagged nanobody is enriched in the pro-oocytes at both stages and gradually became preferentially concentrated in one pro-oocyte (fig. S1A–S1A″). Co-labeling with the synaptonemal complex marker C(3)G confirmed that Msps-EGFP accumulated in pro-oocytes and oocytes undergoing meiosis in regions 2a, 2b, and 3 (fig. S1B–S1C).

Notably, in some cysts, both pro-oocytes are in meiosis, yet only one showed strong Msps enrichment (fig. S1D–S1E), suggesting a transitional phase in which Msps accumulation precedes the eventual selection of a single oocyte.

In summary, both *msps* mRNA and Msps protein are enriched in pro-oocytes and early oocytes, indicating that Msps may act as an early determinant of oocyte specification.

Msps is required for oocyte specification

As Msps is essential for spindle assembly and mitotic progression (*36*), early germline knockdown using the strong driver *nanos (nos)-Gal4*$^{[VP16]}$ (*40, 41*) eliminates the germline entirely (*30*). To bypass this germless phenotype, we employed a weaker *nos-Gal4* line (lacking the VP16 activation domain) in combination with the temperature-sensitive *tub-Gal80[ts]* (*42, 43*). At 18°C, Gal80[ts] suppresses transgene expression in germline cells (OFF), whereas at 30°C, Gal80[ts] is inactivated, allowing germline-specific transgene expression (ON) (Fig. 2A).

We first validated the efficiency of the temperature-sensitive Gal80[ts] system using a nuclear GFP reporter (*UASp-sfGFP-NLS*). Shifting flies from 18°C to 30°C was sufficient to induce robust GFP expression in germline cells (Fig. 2B–2C′).

Having validated that the temperature-sensitive Gal80[ts] system efficiently induces transgene expression upon temperature shift, we next used it to induce the expression of *msps-RNAi*. After shifting adult females from 18°C to 30°C, we observed progressive defects. After 4–6 days, many ovarioles lost their germaria due to impaired

germline cell divisions (Fig. 2D–2F), while the egg chambers that formed showed striking specification defects. In these chambers, Orb frequently failed to accumulate, and a diploid oocyte nucleus was not detected (Fig. 2D–2E' and 2G). By contrast, flies carrying *tub-Gal80[ts]* but lacking *msps-RNAi* showed no detectable defects in germarium maintenance or oocyte specification after 6 days at 30 °C (Fig. 2F–2G), confirming that the observed phenotypes are due to loss of *msps*. Most *msps-RNAi* affected egg chambers contained 16 polyploid nurse cells, consistent with a complete failure of oocyte specification rather than defective cyst formation (Fig. 2D''-2E'' and 2H; movies S2–S3). This phenotype is distinct from the oocyte fate maintenance defects we previously reported in *msps-RNAi* driven by a later germline-specific driver (*maternal αtub-Gal4*$^{[V37]}$), in which egg chambers contain 15 polyploid nurse cells and a single diploid oocyte that progressively loses Orb enrichment during development (*30*). In the *nos-Gal4*–driven *msps-RNAi* samples analyzed here, we also observed a small fraction of egg chambers with 15 polyploid nurse cells and one diploid oocyte lacking Orb enrichment (Fig. 2H), indicating that *msps* depletion predominantly disrupts oocyte specification and can additionally compromise oocyte fate maintenance. This is consistent with our prior findings and underscores that Msps is required both for the initial specification of the oocyte and for subsequent maintenance of oocyte fate.

Furthermore, we employed a blue-light–inducible degradation module (BLID) in which the *Avena sativa* LOV2 domain cages a C-terminal four-amino acid peptide degron (RRRG) in the dark; upon blue-light exposure, unfolding of the LOV2 Jα helix exposes the degron and triggers proteasome-mediated degradation of the fused protein (*44, 45*). We generated a transgene encoding full-length Msps containing RNAi-

resistant silent mutations and fused the BLID module to its C-terminus (fig. S2A). As previously reported, *msps-RNAi* driven by the early, strong *nos-Gal4*$^{[VP16]}$ driver produced a germless phenotype (*30*) (fig. S2B–S2C). In darkness, expression of BLID-tagged Msps fully rescued this phenotype, yielding morphologically normal ovaries and fertile females (fig. S2D–S2E; *nos*$^{[VP16]}$*-Gal4>msps-RNAi* + *Msps-FL-BLID*, hereafter referred to as “Msps-BLID”). By contrast, prolonged blue-light exposure converted these rescued ovaries to a germless phenotype, indicating efficient blue-light-induced Msps degradation (fig. S2F–S2G). Importantly, after a shorter illumination regimen (4 days of blue-light exposure), a substantial fraction of ovarioles exhibited loss of the germarium and loss of oocyte specification, compared with genetically identical samples maintained in darkness and with control samples exposed to the same blue-light regimen (fig. S2H–S2N). Notably, Orb enrichment was absent in the remaining germarium (regions 2b–3) (fig. S2H′ and S2K′) and in early egg chambers (fig. S2J and S2K), consistent with oocyte specification defects.

To disrupt Msps function using an RNAi-independent approach, we introduced an auxin-inducible degron (AID) at the endogenous *msps* locus via CRISPR knock-in, producing Msps-EGFP-AID. To minimize basal degradation in the absence of auxin, a minimal AID tag miniIAA7 was used, and auxin-dependent degradation was enabled by constitutive expression of the cognate *Arabidopsis thaliana* auxin receptor F-box protein AFB2 (AtAFB2) under the *α-tubulin 84B* promoter (*46*) (fig. S3A).

Upon auxin feeding of adult females, the Msps-EGFP signal was efficiently lost in early egg chambers. This depletion was accompanied by a failure of Orb enrichment in region 3/stage 1 egg chambers (fig. S3B–S3E). Auxin treatment also caused defects in

follicle cell divisions and epithelial integrity, and resulted in dying egg chambers at later stages (fig. S3B–S3E), consistent with the essential role of Msps in mitosis. Nevertheless, the early and penetrant loss of oocyte specification provides independent and convergent evidence that Msps is required for oocyte specification.

Altogether, three independent perturbation approaches, temperature-controlled *msps* knockdown and blue-light– or auxin-induced Msps degradation, clearly demonstrate that Msps is essential for oocyte specification.

Msps and Patronin are interdependent in oocyte localization

The microtubule minus-end–binding protein Patronin, the sole *Drosophila* member of the CAMSAP family, is required for symmetry breaking in pro-oocytes and thus for oocyte specification (*7*). To test whether Msps and Patronin act together, we first examined their localization simultaneously. smiFISH staining of *msps* mRNA in ovaries expressing endogenously tagged Patronin-YFP (*29*) revealed co-accumulation of *msps* mRNA and Patronin protein as early as in region 2a, and it persisted throughout the germarium (Fig. 3A–A″). Similarly, Msps-EGFP in ovaries with endogenously tagged Patronin-mKate (*7*) showed Msps-EGFP comets emerging from Patronin-mKate foci in the earliest oocytes (Fig. 3B–3C''; movie S4). These results suggest that Msps and Patronin function in concert during oocyte specification.

To test their interdependence, we perturbed each protein and examined the localization of the other. In *msps-RNAi* ovaries, Patronin-GFP failed to accumulate, accompanied by loss of oocyte specification, as indicated by absent Orb enrichment

and the lack of a diploid oocyte nucleus (Fig. 3D–3F). Conversely, in *patronin* null mutant clones (*patr[c9-c5]*), oocyte specification was disrupted, consistent with the previous report from the St Johnston's lab (*7*), and Msps-EGFP accumulation was lost in homozygous clones but maintained in heterozygous and control clones (Fig. 3G–3I; fig. S4A–S4D). These results indicate that Msps and Patronin are both essential for oocyte specification. Loss of either component disrupts the localization of the other and results in failure of oocyte specification. However, it remains unclear whether this reflects a direct protein-protein interaction or an indirect consequence of failed oocyte selection.

Furthermore, we uncovered a genetic interaction between Msps and Patronin. Having one endogenous copy of Msps tagged with EGFP partially rescued the oocyte specification defects in *patronin* mutant clones, albeit to a limited extent, as indicated by Orb enrichment (magenta arrowheads, Fig. 3G' and fig. S4C–S4D). By contrast, adding an extra copy of GFP-tagged Patronin (*ubi-Patronin-GFP*) enhanced the severity of *msps*-RNAi phenotypes (fig. S4E). These results indicate that Msps and Patronin are functionally interdependent but not equivalent. Although both are required for oocyte specification, altering the dosage or stability of one component modulates the penetrance of defects caused by perturbation of the other, consistent with their distinct and non-redundant functions in the organization of the polarized microtubule network.

Msps is sufficient to promote initial oocyte specification

Having shown that Msps and Patronin are interdependent, we next asked which of them acts upstream. In *msps*-RNAi ovaries, we occasionally observed Patronin

accumulation in germline cells that nevertheless lacked both Orb enrichment and a diploid oocyte nucleus carrying karyosome formation (magenta arrowheads, fig. S4F–F″), suggesting that Patronin accumulation is insufficient to specify an oocyte without Msps. We therefore tested whether ectopic accumulation of Msps is sufficient to initiate oocyte specification.

Oocytes normally exhibit higher microtubule polymerization activity than their sibling nurse cells (*7, 13*). This activity is dependent on Msps accumulation in the oocyte (*30*). Elevated microtubule polymerization activity in the oocyte establishes a polarized microtubule network, with minus-ends concentrated in the oocyte and plus-ends extending into nurse cells through the ring canals, thereby enabling dynein to transport and concentrate oocyte determinants to the oocyte. We reasoned that ectopic recruitment of Msps in nurse cells would increase local microtubule growth, potentially altering the microtubule polarity and concentrating oocyte fate determinants outside of the oocyte.

To achieve this, we developed an optogenetic system, OptoMsps, to recruit Msps onto microtubules via blue light illumination (Fig. 4A). This strategy combines the improved light-induced dimer (iLID) system (*47*) with the NanoTag–nanobody system (*39*). The iLID module consists of an *Avena sativa* LOV2 domain fused to an SsrA peptide, which is sterically blocked in the dark but uncaged by blue light, enabling high-affinity binding to SspB. For microtubule anchoring, we adapted a component of the Opto-Katanin system (*48*), using the N-terminal microtubule-binding domain of EB3, homologous to the *Drosophila* EB-SUN protein (*49*), fused to the blue light–sensitive homo-dimerization module VVDfast (*50*), followed by the iLID (LOV2-SsrA) domain.

Upon blue light exposure, EB3N rapidly dimerizes, increasing its affinity for microtubules, while the SspB–nanobody fusion recruits endogenously tagged Msps to microtubules via the interaction between SsrA and SspB. In this way, local illumination recruits Msps from the oocyte into neighboring nurse cells, where it can enhance microtubule polymerization (Fig. 4B).

We first validated OptoMsps in *Drosophila* S2R+ cells. Local blue light stimulation induced rapid accumulation of Msps-3XTagRFP-3XVHH05 on microtubules (Fig. 4C–4F; movie S5), confirming efficient recruitment of Msps by the OptoMsps system. Notably, the recruited signal often spread beyond the original illuminated region (Fig. 4C-4D), likely due to light scattering and the intrinsic ability of Msps to track growing microtubule ends once recruited.

We next tested OptoMsps in *Drosophila* egg chambers. Global illumination showed rapid recruitment of the OptoMsps components to microtubules within a couple of seconds in nurser cells (fig. S5A–A”; movie S6). To measure functional consequences of Msps recruitment, we used EB1-RFP as a readout of microtubule polymerization activity. Although individual EB1 comets could not be resolved under optogenetic imaging conditions, local Msps recruitment consistently increased EB1-RFP signal in the illuminated area (Fig. 4G–G″; movie S7). Due to the geometry of the nurse cells and the spreading nature of the OptoMsps, the recruitment typically involved two to three nurse cells rather than a single target cell. Nevertheless, blue light stimulation consistently produced a clear increase in EB1-RFP signal, which subsequently spread throughout the entire nurse cell cytoplasm (Fig. 4G–4I).

Finally, we asked whether Msps recruitment could alter oocyte fate markers. Using a MiMIC-based system (*51*), we generated an endogenous tagged Orb-TagRFP line, which completely recapitulates Orb antibody staining and is fully functional as it supports normal oocyte specification when *in trans* with the *orb* null allele (fig. S5B–S5D''). Using this reporter, we found that local Msps recruitment in nurse cells induced a consistent increase in Orb signal, whereas unstimulated nurse cells showed no change over time (Fig. 4J–4K'; movie S8). Quantification confirmed a consistent post-stimulation increase of Orb-TagRFP in the nurse cells upon OptoMsps recruitment (Fig. 4L–4M).

Together, these results demonstrate that targeted recruitment of Msps is sufficient to enhance local microtubule polymerization and promote Orb accumulation in nurse cells, suggesting that Msps activity can initiate key molecular events of oocyte specification.

Asymmetric segregation of Msps protein and dynein-dependent transport of its mRNA

Having established that Msps is both necessary and sufficient for the initiation of oocyte specification, we next asked how the initial Msps asymmetry arises in the pro-oocytes and how it is propagated to a definitive fate decision.

Using two CRISPR knock-in lines (Msps-3XVHH05 and Msps-EGFP), we observed Msps association with the spectrosome and fusome in GSCs, CBs, and early cysts (Fig. 5A; fig. S6A). In later cysts, Msps appeared diffusely enriched around the

branched fusome (Fig. 5A; fig. S6B). From region 2b to region 3, Msps concentrated either in both pro-oocytes or in the presumptive oocyte (fig. S6C–S6E), coinciding with the loss of clear fusome association. Since pro-oocytes are known to inherit more fusome material than their siblings (*5, 52*), it is likely that the spectrosome and fusome association biases Msps segregation toward the pro-oocytes. Supporting this idea, the spectrosome/fusome association of Msps was completely lost when the essential fusome component Hts was depleted by RNAi (fig. S6F–S6H). These findings suggest that Msps asymmetry in cystocytes is established, at least in part, through its association with the spectrosome and fusome structures.

In addition to this protein-level segregation, we asked whether *msps* mRNA is actively targeted to the oocyte by dynein-mediated transport. Previously, we showed that *msps* mRNA accumulation in mid-stage oocytes requires dynein and the mRNA-binding adaptor Egalitarian (Egl) (*30*). Egl functions as the adaptor that links specific mRNAs to BicD and the dynein motor (*53-55*). Here, we examined the interaction between *msps* mRNA and the cytoplasmic dynein complex. Immunoprecipitation of ovarian lysate with Egl antibody showed enrichment of *msps* mRNA compared to control (Fig. 5B), indicating that *msps* mRNA specifically associates with the dynein complex via Egl. Furthermore, we confirmed the role of dynein in *msps* mRNA transport by knocking down the dynein heavy chain (Dhc64C) in the germline using *osk-Gal4*$^{[VP16]}$. We chose *osk-Gal4*$^{[VP16]}$ rather than *nos-Gal4*$^{[VP16]}$ to avoid mitotic defects from dynein depletion in dividing germline stem cells and early cysts, as *osk-Gal4*$^{[VP16]}$ initiates expression in region 2b, after germline cyst divisions are complete, and becomes robust in stage 1 egg chambers (fig. S6I-S6J). In these *osk>Dhc64C-RNAi* samples, *msps*

mRNA lost its oocyte enrichment as early as stages 2–3 (Fig. 5C–5D), although we still detected *msps* mRNA accumulation in pro-oocytes and oocytes through stage 1, consistent with the onset of the *osk-Gal4*$^{[VP16]}$ expression pattern (fig. S6I). Altogether, our data demonstrate that *msps* mRNA is a *bona fide* dynein cargo.

Discussion

In this study, we demonstrate that the conserved microtubule polymerase Msps/XMAP215 is necessary and sufficient to initiate oocyte specification programs in *Drosophila*. Msps accumulates in pro-oocytes and early oocytes (Fig. 1), and its loss abolishes oocyte specification (Fig. 2). Msps and the microtubule minus-end binding protein Patronin are interdependent for oocyte localization and specification (Fig. 3). Using optogenetic recruitment, we further show that increasing Msps activity outside the oocyte is sufficient to induce microtubule polymerization and accumulation of oocyte fate markers (Fig. 4). Finally, we find that Msps protein segregates with the fusome and that *msps* mRNA is transported by the dynein motor complex, allowing its asymmetric enrichment in the oocyte (Fig. 5).

Together, these findings support a positive feedback model in which Msps and dynein cooperate to amplify small initial asymmetries into a definitive oocyte fate. In this model: (1) the future oocyte inherits slightly more Msps protein and microtubule-minus-ends than its sibling pro-oocyte, leading to more microtubule growth with plus-ends out; (2) dynein transports more *msps* mRNA into this cell; and (3) more translated Msps protein further promotes more polarized microtubule assembly, which in turn drives even more dynein-dependent *msps* mRNA transport into the future oocyte. Through this positive feedback loop, an initial small bias in Msps and microtubule polarity is progressively amplified, leading to a robust oocyte specification decision (Fig. 5E).

Oocyte selection: ‘predetermined’ or ‘stochastic’?

Two prevailing models have been proposed to explain how the oocyte is selected. The first ‘predetermined’ model is that the oocyte is specified at the time of the first mitotic division of the cystoblast (in one of the pro-oocytes), and this asymmetry is maintained in subsequent development to a final oocyte selection. The second ‘stochastic’ model assumes that cell competition between the two pro-oocytes results in random selection of the future oocyte by the accumulation of oocyte-specific mRNAs, proteins, and/or organelles (*8*). In both models, the inheritance of fusome materials is the key to the establishment of asymmetry. A later paper from the Stanislav Shvartsman group carefully examined the fusome topology during development, and they found that fusome asymmetry between the pro-oocytes decreases with each cell division, while asymmetry between the pro-oocytes and the rest of the cyst increases (*5*). Thus, they propose the model of ‘equivalency with a bias’: the amplified fusome asymmetry between the pro-oocytes and the other sister cells chooses these two cells as candidates for oocyte selection; decreasing fusome asymmetry between the two pro-oocytes suggests that the oocyte selection between them is likely to be stochastic (*5*).

Our data best fit the ‘equivalency with a bias’ model, where fusome inheritance ensures both pro-oocytes are candidates, but Msps-dynein feedback resolves the competition stochastically. Msps, as a critical oocyte-selection factor, is not simply predetermined or stochastic. Because the fusome extends through intercellular bridges and is partitioned unequally during successive divisions, pro-oocytes inherit more fusome material than their sibling cystocytes (Fig. 5A). Through the Msps-fusome association, they also reliably inherit more Msps, making them the primary candidates for oocyte fate. Subsequently, a small stochastic difference in Msps levels between the

two pro-oocytes is sufficient to start the positive feedback loop that drives a definitive oocyte fate decision. Furthermore, we noticed that Msps is more diffuse around fusome at the later cyst stages and is not clearly associated with fusome in the region 2b pro-oocytes (fig. S6). These observations suggest that stochastic differences between the two pro-oocytes may emerge in region 2a, where the Msps–dynein positive feedback loop could then be engaged to amplify this initial asymmetry.

Oocyte selection: flexible yet robust

Our data showed that *msps* mRNA is a cargo for the dynein motor complex. It binds to dynein through the interaction with the RNA-binding protein Egl and accumulates in the oocyte (Fig. 5) (*30*). Intriguingly, the interaction between *msps* mRNA and Egl is less robust compared to other dynein mRNA cargoes, such as *gurken (grk)* and *nanos (nos)*. One contributing factor may be stage specificity: whereas *grk* and *nos* remain dynein cargos throughout oogenesis, *msps* mRNA functions mainly in early-to-mid stages for oocyte specification and fate maintenance. Because our immunoprecipitation assays used whole-ovary lysates, in which late-stage egg chamber materials are overrepresented, the developmental timing of *msps* transport may reduce the apparent strength of the *msps*–Egl interaction compared to *grk* and *nos*.

In addition, the relatively weak interaction may serve a functional purpose. The development proceeds relatively slowly in the germarium, where ~4 days are required to reach region 3/stage 1, compared to the ~3–4 days needed for the subsequent maturation of egg chambers through stages 1–14 (*56*). We propose that the relatively

weak interaction between *msps* mRNA and the dynein motor complex allows Msps accumulation to build gradually, slowing the amplification of the positive feedback loop. This delay ensures that the commitment to oocyte fate is not made prematurely but instead occurs at the appropriate developmental stage in the germarium.

Interestingly, unlike most other Egl-dependent mRNAs, which typically carry a single RNA stem-loop localization signal (e.g., TLS in *K10*, GLS in *gurken*, ILS in the *I-factor* retrotransposon, and SL1 in *hairy*) (*53, 57-59*), *msps* mRNA contains multiple dynein localization elements distributed in both its coding sequence and 3′UTR (*30*). We propose that this unusual redundancy enhances the robustness of *msps* transport into the oocyte, ensuring reliable activation of the positive feedback loop and enforcing the specification of only one oocyte per cyst.

Positive feedback loops are a recurring theme in oocyte specification. Orb, the *Drosophila* homolog of Cytoplasmic Polyadenylation Element-Binding protein (CPEB), binds to cytoplasmic polyadenylation elements in its own 3′UTR to promote translation of *orb* mRNA, thereby reinforcing Orb accumulation specifically in the oocyte (*25, 60*). This self-sustaining mechanism ensures that once Orb begins to enrich in one cell, it is stabilized and amplified to consolidate oocyte fate. Notably, Orb accumulation becomes predominant in pro-oocytes only in late region 2b, whereas *msps* mRNA and protein are already enriched in region 2a and early region 2b (Fig. 1 and fig. S1). We therefore speculate that the Msps–dynein positive feedback loop acts earlier, followed by the Orb–*orb* positive feedback loop, and that together these mechanisms reinforce the robustness of oocyte specification to ensure that a single cell is selected from each cyst.

Oocyte selection: Microtubule plus- and minus-end regulation

Microtubule organization is central to oocyte selection, requiring a coordinated balance between polymerization at plus-ends and stabilization at minus-ends. Msps/XMAP215, a conserved microtubule polymerase, promotes plus-end growth by accelerating tubulin addition, while Patronin/CAMSAP stabilizes microtubule minus-ends against depolymerization. It is therefore not surprising that both proteins are required and work in concert for oocyte specification, as each contributes to the establishment of the polarized microtubule network that is required for dynein-mediated transport of oocyte determinants.

Intriguingly, our genetic interaction results further illuminate how Msps and Patronin cooperate during oocyte specification. While loss of either protein disrupted the localization of the other and impaired oocyte specification, their dosage sensitivities differ: tagging one endogenous copy of Msps with EGFP provides a partial, but limited, rescue of the oocyte specification defects in *patronin* null clones, as indicated by Orb accumulation; introducing an extra copy of GFP-tagged Patronin driven by a weak ubiquitous promoter (*ubi-Patronin-GFP*) further enhances the defects caused by *msps-RNAi* (fig. S4). These findings point to an asymmetric functional relationship between Msps and Patronin within the polarized microtubule network.

Msps, as a microtubule plus-end polymerase, appears to be rate-limiting for network amplification: increasing Msps levels can partially compensate for reduced minus-end stabilization in *patronin* mutant clones, consistent with the idea that robust plus-end growth can, to some extent, overcome weakened anchoring of microtubule minus-ends. In contrast, elevating Patronin levels in the context of reduced Msps

activity exacerbates oocyte specification defects, suggesting that excessive minus-end stabilization may be detrimental when plus-end polymerization is limiting. Elevating Patronin levels likely increases the number of stabilized microtubule seeds, thereby diluting a limited pool of Msps and preventing individual microtubules from reaching the growth threshold required for network amplification. In addition, over-stabilization may reduce microtubule turnover and plasticity, impairing the reorganization and polarity reinforcement necessary for dynein-driven transport and oocyte fate specification.

Together, these observations argue that oocyte specification does not simply require the presence of both factors, but instead depends on a balance between minus-end stabilization and plus-end polymerization. Disrupting this balance, either by limiting microtubule growth or by over-stabilizing minus ends, compromises the polarized microtubule network required to support dynein-dependent transport and reinforce oocyte fate. These observations highlight the importance of coordinated regulation at both microtubule ends to ensure robust oocyte specification.

Finally, our findings underscore the need for caution when interpreting results from fluorescently tagged proteins, as bulky tags such as GFP can alter protein stability or protein–protein interactions. CRISPR-based tagging strategies using smaller epitopes or nanotags may help to minimize these potential artifacts.

Oocyte selection: conserved principles, divergent structures

Oocyte specification relies on conserved principles of cytoskeletal polarization and the selective accumulation of cell fate determinants; yet, the molecular machinery

guiding this process exhibits both conservation and divergence across species. In *Drosophila*, the Msps/XMAP215–dynein positive feedback loop is embedded within the context of the spectrosome and fusome, organelles unique to insects and other invertebrates that organize the polarized microtubule network, and bias material transfer into the pro-oocytes. In *Xenopus laevis*, recent work described an asymmetric fusome-like structure enriched in stable microtubules and membranous organelles during cyst development (*61*). By contrast, mammalian germline cysts are generally described as lacking fusomes and instead rely on TEX14-stabilized intercellular bridges (*62*).

Despite these structural differences, the overall logic is similar: germline cells undergo incomplete cytokinesis and remain interconnected by intercellular bridges, through which sister cells transfer cytoplasmic materials to a single dominant oocyte (*63*). Recent work has highlighted that centralspindlin and Ect2, core components required for stable intercellular bridges, are evolutionarily conserved across Metazoa, underscoring their dual importance in the emergence of multicellularity and in the maintenance of germline cyst connectivity (*64*). In both fly and mammalian systems, “nurse-like” cells donate cytoplasmic contents, such as mitochondria, Golgi, RNAs, and other organelles, via a microtubule-dependent manner, to support the future oocyte, before undergoing programmed cell death (*13, 14, 65-69*).

Importantly, the central players of the Msps-dynein feedback loop are deeply conserved. The XMAP215 family of microtubule polymerases includes Stu2/Alp14 in yeast, ZYG-9 in *C. elegans*, Msps in *Drosophila*, XMAP215 in *Xenopus*, and ch-TOG/CKAP5 in mammals and humans (*70*). Dynein is likewise conserved as the primary minus-end motor that transports a diverse array of cargos, including mRNAs

and organelles, across eukaryotes (*71-73*). Consistent with this conserved role, studies in mouse germline cysts have shown that dynein activity is required for the transfer of cytoplasmic contents, including mitochondria, Golgi, and RNAs, from sister cells into the future oocyte, a process essential for its growth and survival (*65, 67*).

Whether ch-TOG/CKAP5 contributes directly to mammalian oocyte selection remains unknown. If so, one would expect asymmetric enrichment of CKAP5 before bridge collapse, localized microtubule growth biasing plus-ends away from the future oocyte, and altered oocyte selection upon CKAP5 perturbation. Because ch-TOG is also essential for spindle assembly (*74*), future studies using temporally controlled degradation or optogenetic approaches will be required to uncouple these roles.

Summary

In summary, our study identifies Msps/XMAP215 as a key upstream regulator of oocyte specification in *Drosophila*. We demonstrate that Msps is both necessary and sufficient for the initiation of the oocyte specification programs: loss of Msps abolishes oocyte specification, while optogenetic recruitment of Msps is sufficient to trigger it. By coupling dynein-mediated mRNA transport with microtubule polymerization, Msps establishes a positive feedback loop that ensures robust oocyte selection. These findings illustrate how germline cysts amplify a small initial asymmetry to reliably select a single oocyte from a syncytial cyst.

Materials and Methods

***Drosophila* Husbandry and Maintenance.** Fly stocks and crosses were maintained on standard cornmeal food (Nutri-Fly Bloomington Formulation, Genesee, Cat. #66-121) supplemented with active dry yeast at 25 °C, except for temperature-sensitive experiments, which were conducted at the specific temperatures indicated.

The following flies were used in this study: *UAS-msps-RNAi* (HMS01906, attP40, II, Bloomington *Drosophila* Stock Center (BDSC) # 38990, targeting Msps CDS 5001-5021 nt, 5'- CTGCGCGACTATGAAGAAATA-3') (RRID:BDSC_38990) (*30, 75*); *nos-Gal4*$^{[VP16]}$ (III)(*40, 41*); *ubi-GFP-Pav* (II, from Dr. David Glover, Caltech)(*76*); *nos-Gal4*$^{[no\ VP16]}$ (II); *tub-Gal80[ts]* (III) (from Dr. Yukiko Yamashita, Whitehead Institute, MIT); *UASp-Msps (RNAi-resistant)-YFP-BLID (55C4, attP1, II) (30)***;** *w*$^{[1118]}$ (X, BDSC # 5905; RRID:BDSC_5905); *osk-Gal4*$^{[VP16]}$ (III, BDSC # 44242; RRID:BDSC_44242); *Orb-GFP* (BDSC # 59817; RRID:BDSC_59817) and *MiMIC Orb*$^{[MI04761]}$ (BDSC # 37978; RRID:BDSC_37978) (*77*); *Patronin-YFP* (II, CRISPR knockin) (*29*), *Patronin-mKate* (II, CRISPR knockin), *ubi-Patronin.RA-GFP* (X), *FRT G13 patr*$^{[C9-C5]}$ (II) , and *UASp-EB1-RFP* (III, attP2) (*7*) (from Dr. Daniel St Johnston, University of Cambridge); *Tub-PBac* (BDSC #8285; BDSC_8285); *UASt-NbVHH05-EGFP* (attP40, II, BDSC # 94008; RRID:BDSC_94008) (*39*); *hs-FLP*$^{[12]}$ (X, BDSC # 1929; RRID:BDSC_1929); *FRT G13* (II, BDSC #1956; RRID:BDSC_1956); *FRT G13 ubi-GFP.nls(2R1) ubi-GFP.nls(2R2)* (II, BDSC # 5826; RRID:BDSC_5826); *UASp-sfGFP-NLS* (III) (*78*); *orb*$^{[F343]}$ (BDSC # 58477; RRID:BDSC_58477)(*79, 80*); *UAS-Dhc64C-RNAi* (TRiP.GL00543, attP40, II, BDSC #36583, targeting DHC64C CDS 10044–10,064 nt, 5'-TCGAGAGAAGATGAAGTCCAA-3')(RRID:BDSC_36583) (*14, 75, 81, 82*).

The following lines were generated in this study (by BestGene Inc.): *UASp-NbVHH05-3XTagRFP* (*attP14*, 36A10, PhiC31-mediated integration); *UASp-EB3N-VVDfast-mClover3-iLID* (*attP14*, 36A10, PhiC31-mediated integration); *UASp-NbVHH05-GFP-SspB* (VK22, 57F5, PhiC31-mediated integration); *Msps-EGFP-AID* (CRISPR knock-in); α*tub84B promoter-AtAFB2* (attP1, 55C4, PhiC31-mediated integration), *Orb-TagRFP-3XHA* (MiMIC insertion).

Plasmid Constructs.

<u>-pUASp-attB-NbVHH05-3XTagRFP:</u> NbVHH05 (the alpaca nanobody against VHH05 nanotag) was PCR-amplified from pAW-NbVHH05-GFP (Addgene Plasmid #171570)(*39*) and subcloned into pUASp-attB-EMTB-3XTagRFP (*83*) via EcoRI(5')/SpeI(3'), replacing EMTB with NbVHH05.

<u>-pUASp-attB-EB3N-VVDfast-mClover3-iLID:</u> EB3N-VVDfast-mClover3-iLID was PCR-amplified from pB80-EB3(1-189)-VVDfast-mClover3-iLID (a gift from Dr. Anna Akhmanova, Utrecht University) (*48*) and cloned into pUASp-attB via SpeI(5')/PspXI(3').

<u>-pUASp-attB-NbVHH05-GFP-SspB:</u> GFP-SspB was subcloned from pUASp-GFP-SspB (*83*) to replace 3XTagRFP in pUASp-attB-NbVHH05-3XTagRFP via SpeI(5')/BamHI(3')

<u>-pUASp-Msps-3XTagRFP-3XVHH05:</u> The 3XVHH05 tag was PCR-amplified from pScarlessHD-3XVHH05-6XMS2-DsRed (*30*) and inserted into pUASp-attB-3XTagRFP (*83*) via BamHI(5')/XbaI(3'). An RNAi-resistant Msps (with silent mutations in the *msps-RNAi* target sequence) was subcloned from pUASp-attB-Msps(RNAi-resistant)-YFP-BLID-K10.TLS (*30*) into pUASp-attB-3XTagRFP-3XVHH05 via NotI(5')/SpeI(3').

-pScarlessHD-5′ *msps* homology arm-C-EGFP-AID-DsRed-3′ *msps* homology arm: the construct was generated by Epoch Life Science by inserting the 5′ *msps* homology arm, EGFP, miniIAA7 (AID), DsRed, and the 3′ *msps* homology arm in the pScarlessHD-C-3xVHH05-DsRed (Addgene, Plasmid #171580; RRID:Addgene_171580) to replace 3XVHH05-DsRed by infusion cloning.

-pattB-αtub84B promoter-AtAFB2-Myc: A codon-optimized *AtAFB2* sequence for *Drosophila*, fused to a C-terminal Myc tag and followed by the *α-tubulin 84B* 3′ UTR and SV40 polyadenylation signal, was synthesized and inserted into the pattB vector (DGRC 1420; RRID:DGRC_1420) via EcoRI (5′) and XbaI (3′) restriction sites to generate pattB-AtAFB2-Myc. The *Drosophila α-tubulin 84B* promoter was amplified from the pattB-tub-AtTIR1-P2A-AID-GAL80-AID plasmid (DGRC #1568; RRID:DGRC_1568) and inserted upstream of *AtAFB2-Myc* using BamHI (5′) and EcoRI (3′) sites, creating pattB-αtub84B promoter-AtAFB2-Myc.

CRISPR Knock-In to Create Msps-EGFP-AID. The plasmid pScarlessHD-5′ *msps* homology arm-C-EGFP-AID-DsRed-3′ *msps* homology arm was co-injected with two previously described gRNAs cloned in the pCFD5 vector (gRNA #1: GGGGTATTTCAATCAGAAGC; gRNA #2: ACGGGAAGCGCACAGTTTAT) (*30*) into *yw; nos-Cas9 attP40*/*CyO* flies by BestGene Inc. Progeny carrying the knock-in were identified by DsRed eye fluorescence and subsequently crossed to *Tub-PBac* flies to excise the DsRed marker via PBac transposase.

Generation of Orb-TagRFP-3XHA Protein Trap Line via Minos Mediated Integration Cassette (MiMIC) and Recombinase Mediated Cassette Exchange (RMCE). A

protein-trap cassette intron DNA construct (DGRC, #1301, pBS-KS-attB1-2-PT-SA-SD-0-TagRFP-T-3xHA, phase 0; RRID:DGRC_1301) was injected into the MiMIC line *Orb[MI04761]* (BDSC # 37978; RRID:BDSC_37978) (*51*) in the presence of phiC31 integrase by BestGene Inc. (fig. S5B). Transformants were identified by loss of body pigmentation (*yellow+*), and correct cassette orientation was confirmed by TagRFP expression in the ovary.

Immunostaining in *Drosophila* Egg Chambers. Immunostaining was performed using a standard fixation and staining protocol as previously described (*78, 83, 84*). Young adult females were mated with males and fed active dry yeast for 16–18 h before dissection. Primary antibodies used in this study: mouse monoclonal anti-Orb antibody (Orb 4H8, Developmental Studies Hybridoma Bank/DSHB, supernatant, 1:5; RRID:AB_528418) (*79*); mouse anti-C(3)G antibody (1A8-1G2, 1:500) (*85*); mouse monoclonal anti-Hts antibody (1B1, DSHB, 1:5; RRID:AB_528070) (*86*). Samples were incubated with primary antibodies at 4 °C overnight. Secondary antibodies [FITC-conjugated, TRITC-conjugated, Alexa Fluor 647-conjugated anti-mouse IgG (Jackson ImmunoResearch Laboratories, Inc.; Cat# 115-095-062, RRID: AB_2338594; Cat# 115-025-003, RRID: AB_2338478; Cat# 715-605-150, RRID: AB_2340862)] were used at 10 µg/mL at room temperature (24 – 25 °C) for 4 h. In some experiments, rhodamine- or Alexa Fluor 633-conjugated phalloidin (0.2 µg/mL) and DAPI (1 µg/mL) were included. Samples were mounted in Mowiol mounting medium and dried for two days before imaging.

Single-Molecule Inexpensive Fluorescence *in situ* Hybridization (smiFISH). smiFISH was performed following standard protocols described previously (*30, 43*).

Twenty-five 20-nucleotide-long DNA probes complementary to the 3'UTR of *msps* mRNA were designed, each carrying a 3′ FLAP-X sequence (5′-CCTCCTAAGTTTCGAGCTGGACTCAGTG-3′)(*30*). Probes were mixed at equal molar ratios and annealed with a fluorescently labeled probe carrying 5′ and 3′ Cy5 modifications (/5Cy5/CACTGAGTCCAGCTCGAAACTTAGGAGG-/3Cy5Sp/).

Germline FRT Clone Induction. Virgin females of genotype *FRTG13 ubi-GFP.nls*/*CyO* or *FRTG13 ubi-GFP.nls*/*CyO; Msps-EGFP* were crossed with males carrying *hs-flp*$^{[12]}$*/Y; FRTG13 patr*$^{[C9-C5]}$*/CyO or hs-flp*^{12}*/Y; FRTG13*/*CyO*. From these crosses, young pupae at 7–8 days after egg laying (AEL) were heat shocked at 37°C for 2 hours on two consecutive days. Non-CyO F1 females were collected 3-4 days after heat shock, fattened with active dry yeast overnight, and dissected for Orb staining.

Live Imaging of *Drosophila* Egg Chambers. Young female adults were mated with males and fed active dry yeast for 16 to 18 h before dissection. Ovaries were dissected in Halocarbon oil 700 (Sigma-Aldrich, Cat# H8898) as described previously (*13, 14, 30, 78, 83, 84*). Freshly dissected samples were imaged using a 40×/1.25 N.A. silicone oil lens on a Nikon W1 spinning disk confocal microscope (Yokogawa CSU, pinhole size 50 µm) equipped with a Hamamatsu ORCA-Fusion digital CMOS camera, controlled by Nikon Elements software.

Blue-light-induced Msps protein degradation: F1 flies of *yw; UASp-Msps (RNAi-resistant)-YFP-BLID/UAS-msps-RNAi; nos-Gal4*$^{[VP16]}$/+ or *w*$^{[1118]}$ were raised and kept in darkness (vials wrapped in aluminum foil). Blue-light treatment was performed using an LED blue color light bulb (60 W equivalent) positioned on top of a narrow polypropylene vial containing adult flies (~2 cm above the plug) for the indicated duration prior to

standard ovary dissection, fixation, and staining procedures. Whole-ovary images were acquired on a CICERO spinning disk confocal microscope (CrestOptics) with large-area image stitching, and individual ovariole images were acquired on a Nikon W1 spinning disk confocal microscope; both systems were controlled by Nikon Elements software.

Auxin-induced Msps protein degradation: F1 flies of *yw; αtub84B promoter-AtAFB2 /CyO; Msps-EGFP-AID/Msps-EGFP-AID* were first starved overnight and then divided into two groups. One group was fed yeast paste supplemented with 200 mM indole-3-acetic acid (IAA) sodium salt (Sigma-Aldrich, I5148-2G; diluted in dH_2O), while the control group was fed yeast paste prepared with dH_2O alone. All treatments were performed in the dark to prevent light-induced degradation of IAA, and flies were maintained over the yeast paste at 25 °C for 6 days prior to standard ovary dissection, fixation, and staining procedures.

OptoMsps Recruitment in *Drosophila* S2R + Cells. *Drosophila* S2R+ cells (DGRC Stock #150; RRID: CVCL_Z831) were maintained in Insect-Xpress medium (Lonza, Catalog # 12-730Q) in a 25°C incubator and were transiently transfected with pAC-Gal4, pUASp-EB3N-VVDfast-mClover3-iLID, pUASp-NbVHH05-GFP-SspB, and pUASp-Msps-3XTagRFP-3XVHH05 at a 4:3:3:1 ratio using Effectene (Qiagen, Cat# 301425) following the manufacturer's instructions. After 2-3 days, cells were plated on Concanavalin A (ConA)-coated coverslips and imaged on a Nikon W1 spinning disk confocal microscope (Yokogawa CSU, pinhole size 50 µm) equipped with a Hamamatsu ORCA-Fusion digital CMOS camera and a 100×/1.35 N.A. silicone oil lens, controlled by Nikon Elements software. Optogenetic recruitment was induced by a 470 nm Lumencor LED light controlled by a Mightex Polygon DMD Illuminator at 0.8% power,

with 30 s of continuous illumination per cycle, followed by acquisition using a 561 nm laser at a single focal plane and an end-point final acquisition using a 488 nm laser. All the procedures were performed under red-light-only conditions to minimize unintended activation from ambient light.

OptoMsps Recruitment in *Drosophila* Ovaries with EB1-RFP. Recombination between (1) *UASp-EB3N-VVDfast-mClover3-iLID* (attP14) and *UASp-NbVHH05-GFP-SspB (VK22)*; (2) *osk-Gal4*$^{[VP16]}$ (III) and *Msps-3XVHH05-6XMS2* (89B1-89B2); (3) *UASp-EB1-RFP* (attP2) and *Msps-3XVHH05-6XMS2* (89B1-89B2) were performed following standard protocols. F1 females of *yw*; *UASp-EB3N-VVDfast-mClover3-iLID, UASp-NbVHH05-GFP-SspB*/*CyO; osk-Gal4*$^{[VP16]}$*, Msps-3XVHH05-6XMS2/UASp-EB1-RFP, Msps-3XVHH05-6XMS2* were dissected in Halocarbon oil 700 and imaged on a Nikon W1 spinning disk confocal microscope (Yokogawa CSU, pinhole size 50 µm) equipped with a Hamamatsu ORCA-Fusion digital CMOS camera and a 40×/1.25 N.A. silicone oil lens, controlled by Nikon Elements software. Optogenetic recruitment was induced by a 470 nm Lumencor LED light controlled by a Mightex Polygon DMD Illuminator at 0.8% power, with 30 s continuous illumination per cycle. Imaging was performed using a 561 nm laser at a single focal plane, 2 s intervals for a total of 10 s. For the results, only the first frame of each 10 sec time lapse per illumination cycle was shown (Fig. 4), and the EB1 signal across the entire illuminated nurse cells (not just the illuminated area) was analyzed; sum projections of the full 10 sec time lapses are presented in movie S7. All procedures were performed under red-light-only conditions to prevent unintended activation by ambient light.

OptoMsps Recruitment in *Drosophila* Ovaries with Orb-TagRFP. Recombination between *Msps-3XVHH05-6XMS2* (89B1-89B2) and *Orb-TagRFP* (94E9) was performed following standard protocols. F1 females of *yw*; *UASp-EB3N-VVDfast-mClover3-iLID, UASp-NbVHH05-GFP-SspB/CyO; osk-Gal4*$^{[VP16]}$*, Msps-3XVHH05-6XMS2/Orb-TagRFP , Msps-3XVHH05-6XMS2* were dissected in supplemented Schneider's medium (pH 6.9; 20 mM HEPES, 0.5 mg/mL Bovine Serum Albumin (BSA), 5 mM Glucose, 20% fetal bovine serum (FBS), 5 µg/ml insulin, 100 µg/ml penicillin-streptomycin, 10 µg/ml tetracycline, and 5 µM 20-Hydroxyecdysone) containing 25 µM biliverdin dihydrochloride (MP Biomedicals Cat #194886) for far-red membrane labeling. Ovarioles in supplemented Schneider's medium were mixed with BME hydrogel (R&D Systems, BME001-01) at a volume ratio of 2:1 and mounted in a "sandwich" configuration between a lummox membrane (Sarstedt, # 94.6150.101) and a glass coverslip, using acid-washed ≤106 µm (−140 U.S. sieve) glass beads (Sigma Aldrich, G4649-10G) as the spacer and silicone vacuum grease (Beckman, Product # 335148) as the glue. Samples were allowed to briefly solidify at 30 °C for 15–20 minutes before imaging. Imaging was performed on a Nikon W1 spinning disk confocal microscope (Yokogawa CSU, pinhole size 50 µm) equipped with a Hamamatsu ORCA-Fusion digital CMOS camera and a 40×/1.25 N.A. silicone oil lens, controlled by Nikon Elements software. Local optogenetic recruitment was induced by a 470 nm Lumencor LED light controlled by a Mightex Polygon DMD Illuminator at 0.8% power and continuous illumination for 2 min per cycle, followed by acquisition with 561nm and 640nm lasers over an 18-µm z-stack (3 µm each step, a total of 7 steps). Sum slices of the z-stacks of the entire nurse cells and the oocyte were used for analysis and presentation (Fig. 4;

movie S8). Global optogenetic recruitment was induced by acquisition using a 488 nm laser at 2s intervals for 2 min at a single focal plane (movie S6). All procedures were performed under red-light-only conditions to avoid unintended activation by ambient light.

Egl-mRNA binding assay: The *in vivo* RNA binding experiment was performed as previously described (*54, 87*). In brief, ovarian lysates were prepared from wild-type flies. 600 µg of total lysate was used in each immunoprecipitation, using either an anti-HA antibody (control) or an antibody against Egl. The co-precipitating RNAs were eluted, extracted, and reverse transcribed using Superscript III (Life Technologies). SsoAdvanced Universal SYBR green supermix (BioRad) was used to perform the quantitative PCR reaction using a Bio-Rad CFX96 Real-time PCR machine. Fold enrichment was calculated by normalizing the amount of *msps*, *nos*, and *grk* mRNAs that precipitated with the control anti-HA antibody versus the anti-Egl antibody.

Quantification and Statistics. Figures display either percentages of phenotypes or mean values, as indicated in the figure legends. Error bars represent SEM, and *n* represents the number of samples (cells, ovarioles, or egg chambers, as indicated in the legends) analyzed for each assay. Each experiment was performed in 2–3 independent biological replicates. Biological replicates consisted of ovaries from different flies of the same genotype obtained from independent dissections performed on different days. Data from biological replicates were combined for analysis. Statistical significance was assigned as follows: $P \geq 0.05$, not significant (n.s.); $0.01 \leq P < 0.05$, significant (*); $0.001 \leq P < 0.01$, very significant (**); $0.0001 \leq P < 0.001$, extremely significant (***); $P < 0.0001$, extremely significant (****).

References

1. D. Kirilly, T. Xie, The Drosophila ovary: an active stem cell community. *Cell Res* **17**, 15-25 (2007).
2. H. Lin, L. Yue, A. C. Spradling, The Drosophila fusome, a germline-specific organelle, contains membrane skeletal proteins and functions in cyst formation. *Development* **120**, 947-956 (1994).
3. H. Lin, A. C. Spradling, Fusome asymmetry and oocyte determination in Drosophila. *Dev Genet* **16**, 6-12 (1995).
4. W. Deng, H. Lin, Spectrosomes and fusomes anchor mitotic spindles during asymmetric germ cell divisions and facilitate the formation of a polarized microtubule array for oocyte specification in Drosophila. *Developmental biology* **189**, 79-94 (1997).
5. R. Diegmiller, J. Imran Alsous, D. Li, Y. M. Yamashita, S. Y. Shvartsman, Fusome topology and inheritance during insect gametogenesis. *PLoS computational biology* **19**, e1010875 (2023).
6. S. L. Page, R. S. Hawley, c(3)G encodes a Drosophila synaptonemal complex protein. *Genes Dev* **15**, 3130-3143 (2001).
7. D. Nashchekin, L. Busby, M. Jakobs, I. Squires, D. St Johnston, Symmetry breaking in the female germline cyst. *Science* **374**, 874-879 (2021).
8. T. D. Hinnant, J. A. Merkle, E. T. Ables, Coordinating Proliferation, Polarity, and Cell Fate in the Drosophila Female Germline. *Front Cell Dev Biol* **8**, 19 (2020).
9. V. Lantz, J. S. Chang, J. I. Horabin, D. Bopp, P. Schedl, The Drosophila Orb Rna-Binding Protein Is Required for the Formation of the Egg Chamber and Establishment of Polarity. *Gene Dev* **8**, 598-613 (1994).
10. J. S. Chang, L. H. Tan, P. Schedl, The Drosophila CPEB homolog, Orb, is required for Oskar protein expression in oocytes. *Developmental biology* **215**, 91-106 (1999).
11. A. P. Mahowald, J. M. Strassheim, Intercellular migration of centrioles in the germarium of Drosophila melanogaster. An electron microscopic study. *The Journal of cell biology* **45**, 306-320 (1970).
12. J. Bolivar, J. R. Huynh, H. Lopez-Schier, C. Gonzalez, D. St Johnston, A. Gonzalez-Reyes, Centrosome migration into the Drosophila oocyte is independent of BicD and egl, and of the organisation of the microtubule cytoskeleton. *Development* **128**, 1889-1897 (2001).
13. W. Lu, M. Lakonishok, V. I. Gelfand, Gatekeeper function for Short stop at the ring canals of the Drosophila ovary. *Curr Biol*, (2021).
14. W. Lu, M. Lakonishok, A. S. Serpinskaya, V. I. Gelfand, A novel mechanism of bulk cytoplasmic transport by cortical dynein in Drosophila ovary. *eLife* **11**, (2022).
15. M. Buszczak, L. Cooley, Eggs to die for: cell death during Drosophila oogenesis. *Cell Death Differ* **7**, 1071-1074 (2000).
16. L. Yue, A. C. Spradling, hu-li tai shao, a gene required for ring canal formation during Drosophila oogenesis, encodes a homolog of adducin. *Genes & development* **6**, 2443-2454 (1992).

17. M. de Cuevas, J. K. Lee, A. C. Spradling, alpha-spectrin is required for germline cell division and differentiation in the Drosophila ovary. *Development* **122**, 3959-3968 (1996).
18. W. E. Theurkauf, B. M. Alberts, Y. N. Jan, T. A. Jongens, A central role for microtubules in the differentiation of Drosophila oocytes. *Development* **118**, 1169-1180 (1993).
19. K. Röper, N. H. Brown, A Spectraplakin Is Enriched on the Fusome and Organizes Microtubules during Oocyte Specification in Drosophila. *Current Biology* **14**, 99-110 (2004).
20. D. Nashchekin, I. Squires, A. Prokop, D. St Johnston, The Shot CH1 domain recognises a distinct form of F-actin during Drosophila oocyte determination. *Development* **151**, (2024).
21. M. McGrail, T. S. Hays, The microtubule motor cytoplasmic dynein is required for spindle orientation during germline cell divisions and oocyte differentiation in Drosophila. *Development* **124**, 2409-2419 (1997).
22. B. Ran, R. Bopp, B. Suter, Null alleles reveal novel requirements for Bic-D during Drosophila oogenesis and zygotic development. *Development* **120**, 1233-1242 (1994).
23. T. Schupbach, E. Wieschaus, Female sterile mutations on the second chromosome of Drosophila melanogaster. II. Mutations blocking oogenesis or altering egg morphology. *Genetics* **129**, 1119-1136 (1991).
24. A. Swan, T. Nguyen, B. Suter, Drosophila Lissencephaly-1 functions with Bic-D and dynein in oocyte determination and nuclear positioning. *Nature cell biology* **1**, 444-449 (1999).
25. J. Barr, R. Gilmutdinov, L. Wang, Y. Shidlovskii, P. Schedl, The Drosophila CPEB Protein Orb Specifies Oocyte Fate by a 3'UTR-Dependent Autoregulatory Loop. *Genetics* **213**, 1431-1446 (2019).
26. S. Castagnetti, A. Ephrussi, Orb and a long poly(A) tail are required for efficient oskar translation at the posterior pole of the Drosophila oocyte. *Development* **130**, 835-843 (2003).
27. J. S. Chang, L. Tan, M. R. Wolf, P. Schedl, Functioning of the Drosophila orb gene in gurken mRNA localization and translation. *Development* **128**, 3169-3177 (2001).
28. D. St Johnston, Polarity and axis formation in the Drosophila female germ line. *Curr Top Dev Biol* **154**, 73-97 (2023).
29. D. Nashchekin, A. R. Fernandes, D. St Johnston, Patronin/Shot Cortical Foci Assemble the Noncentrosomal Microtubule Array that Specifies the Drosophila Anterior-Posterior Axis. *Developmental cell* **38**, 61-72 (2016).
30. W. Lu, M. Lakonishok, V. I. Gelfand, The dynamic duo of microtubule polymerase Mini spindles/XMAP215 and cytoplasmic dynein is essential for maintaining Drosophila oocyte fate. *Proceedings of the National Academy of Sciences of the United States of America* **120**, e2303376120 (2023).
31. W. Moon, T. Hazelrigg, The Drosophila microtubule-associated protein mini spindles is required for cytoplasmic microtubules in oogenesis. *Current biology : CB* **14**, 1957-1961 (2004).

32. K. C. Slep, The role of TOG domains in microtubule plus end dynamics. *Biochem Soc Trans* **37**, 1002-1006 (2009).
33. G. J. Brouhard, J. H. Stear, T. L. Noetzel, J. Al-Bassam, K. Kinoshita, S. C. Harrison, J. Howard, A. A. Hyman, XMAP215 is a processive microtubule polymerase. *Cell* **132**, 79-88 (2008).
34. P. O. Widlund, J. H. Stear, A. Pozniakovsky, M. Zanic, S. Reber, G. J. Brouhard, A. A. Hyman, J. Howard, XMAP215 polymerase activity is built by combining multiple tubulin-binding TOG domains and a basic lattice-binding region. *Proceedings of the National Academy of Sciences of the United States of America* **108**, 2741-2746 (2011).
35. A. E. Byrnes, K. C. Slep, TOG-tubulin binding specificity promotes microtubule dynamics and mitotic spindle formation. *The Journal of cell biology* **216**, 1641-1657 (2017).
36. C. F. Cullen, P. Deak, D. M. Glover, H. Ohkura, mini spindles: A gene encoding a conserved microtubule-associated protein required for the integrity of the mitotic spindle in Drosophila. *The Journal of cell biology* **146**, 1005-1018 (1999).
37. C. F. Cullen, H. Ohkura, Msps protein is localized to acentrosomal poles to ensure bipolarity of Drosophila meiotic spindles. *Nature cell biology* **3**, 637-642 (2001).
38. G. Goshima, R. Wollman, N. Stuurman, J. M. Scholey, R. D. Vale, Length control of the metaphase spindle. *Current biology : CB* **15**, 1979-1988 (2005).
39. J. Xu, A. R. Kim, R. W. Cheloha, F. A. Fischer, J. S. S. Li, Y. Feng, E. Stoneburner, R. Binari, S. E. Mohr, J. Zirin, H. L. Ploegh, N. Perrimon, Protein visualization and manipulation in Drosophila through the use of epitope tags recognized by nanobodies. *eLife* **11**, (2022).
40. M. Van Doren, A. L. Williamson, R. Lehmann, Regulation of zygotic gene expression in Drosophila primordial germ cells. *Current biology : CB* **8**, 243-246 (1998).
41. W. Lu, M. O. Casanueva, A. P. Mahowald, M. Kato, D. Lauterbach, E. L. Ferguson, Niche-associated activation of rac promotes the asymmetric division of Drosophila female germline stem cells. *PLoS biology* **10**, e1001357 (2012).
42. S. E. McGuire, G. Roman, R. L. Davis, Gene expression systems in Drosophila: a synthesis of time and space. *Trends in genetics : TIG* **20**, 384-391 (2004).
43. W. Lu, B. S. Lee, H. X. Y. Deng, M. Lakonishok, E. Martin-Blanco, V. I. Gelfand, 'Mitotic' kinesin-5 is a dynamic brake for axonal growth in Drosophila. *Development* **152**, (2025).
44. K. M. Bonger, R. Rakhit, A. Y. Payumo, J. K. Chen, T. J. Wandless, General method for regulating protein stability with light. *ACS Chem Biol* **9**, 111-115 (2014).
45. L. M. Stevens, G. Kim, T. Koromila, J. W. Steele, J. McGehee, A. Stathopoulos, D. S. Stein, Light-dependent N-end rule-mediated disruption of protein function in Saccharomyces cerevisiae and Drosophila melanogaster. *PLoS genetics* **17**, e1009544 (2021).
46. S. Li, X. Prasanna, V. T. Salo, I. Vattulainen, E. Ikonen, An efficient auxin-inducible degron system with low basal degradation in human cells. *Nature methods* **16**, 866-869 (2019).

47. G. Guntas, R. A. Hallett, S. P. Zimmerman, T. Williams, H. Yumerefendi, J. E. Bear, B. Kuhlman, Engineering an improved light-induced dimer (iLID) for controlling the localization and activity of signaling proteins. *Proceedings of the National Academy of Sciences of the United States of America* **112**, 112-117 (2015).
48. J. C. M. Meiring, I. Grigoriev, W. Nijenhuis, L. C. Kapitein, A. Akhmanova, Opto-katanin, an optogenetic tool for localized, microtubule disassembly. *Current biology : CB* **32**, 4660-4674 e4666 (2022).
49. S. K. Kim, S. L. Rogers, W. Lu, B. S. Lee, V. I. Gelfand, EB-SUN, a new microtubule plus-end tracking protein in Drosophila. *Molecular biology of the cell* **35**, ar147 (2024).
50. W. Nijenhuis, M. M. P. van Grinsven, L. C. Kapitein, An optimized toolbox for the optogenetic control of intracellular transport. *The Journal of cell biology* **219**, (2020).
51. K. J. Venken, K. L. Schulze, N. A. Haelterman, H. Pan, Y. He, M. Evans-Holm, J. W. Carlson, R. W. Levis, A. C. Spradling, R. A. Hoskins, H. J. Bellen, MiMIC: a highly versatile transposon insertion resource for engineering Drosophila melanogaster genes. *Nature methods* **8**, 737-743 (2011).
52. M. de Cuevas, A. C. Spradling, Morphogenesis of the Drosophila fusome and its implications for oocyte specification. *Development* **125**, 2781-2789 (1998).
53. M. Dienstbier, F. Boehl, X. Li, S. L. Bullock, Egalitarian is a selective RNA-binding protein linking mRNA localization signals to the dynein motor. *Genes & development* **23**, 1546-1558 (2009).
54. H. Neiswender, C. H. Goldman, R. Veeranan-Karmegam, G. B. Gonsalvez, Dynein light chain-dependent dimerization of Egalitarian is essential for maintaining oocyte fate in Drosophila. *Developmental biology* **478**, 76-88 (2021).
55. J. M. Mach, R. Lehmann, An Egalitarian-BicaudalD complex is essential for oocyte specification and axis determination in Drosophila. *Genes & development* **11**, 423-435 (1997).
56. A. M. Hudson, L. Cooley, Methods for studying oogenesis. *Methods* **68**, 207-217 (2014).
57. T. L. Serano, R. S. Cohen, A small predicted stem-loop structure mediates oocyte localization of Drosophila K10 mRNA. *Development* **121**, 3809-3818 (1995).
58. V. Van De Bor, E. Hartswood, C. Jones, D. Finnegan, I. Davis, gurken and the I factor retrotransposon RNAs share common localization signals and machinery. *Developmental cell* **9**, 51-62 (2005).
59. S. L. Bullock, D. Zicha, D. Ish-Horowicz, The Drosophila hairy RNA localization signal modulates the kinetics of cytoplasmic mRNA transport. *The EMBO journal* **22**, 2484-2494 (2003).
60. L. Tan, J. S. Chang, A. Costa, P. Schedl, An autoregulatory feedback loop directs the localized expression of the Drosophila CPEB protein Orb in the developing oocyte. *Development* **128**, 1159-1169 (2001).
61. A. Davidian, A. C. Spradling, Early female germline development in Xenopus laevis: Stem cells, nurse cells, and germline cysts. *Proceedings of the National Academy of Sciences of the United States of America* **122**, e2522343122 (2025).

62. K. Lu, L. Jensen, L. Lei, Y. M. Yamashita, Stay Connected: A Germ Cell Strategy. *Trends in genetics : TIG* **33**, 971-978 (2017).
63. W. Lu, V. I. Gelfand, Go with the flow - bulk transport by molecular motors. *Journal of cell science* **136**, (2023).
64. M. Glotzer, A key role for centralspindlin and Ect2 in the development of multicellularity and the emergence of Metazoa. *Current biology : CB* **35**, 3251-3262 e3251 (2025).
65. K. Ikami, N. Nuzhat, L. Lei, Organelle transport during mouse oocyte differentiation in germline cysts. *Current opinion in cell biology* **44**, 14-19 (2017).
66. K. Ikami, S. Shoffner-Beck, M. Tyczynska Weh, S. Schnell, S. Yoshida, E. A. Diaz Miranda, S. Ko, L. Lei, Branched germline cysts and female-specific cyst fragmentation facilitate oocyte determination in mice. *Proceedings of the National Academy of Sciences of the United States of America* **120**, e2219683120 (2023).
67. L. Lei, A. C. Spradling, Mouse oocytes differentiate through organelle enrichment from sister cyst germ cells. *Science* **352**, 95-99 (2016).
68. W. Niu, A. C. Spradling, Mouse oocytes develop in cysts with the help of nurse cells. *Cell* **185**, 2576-2590 e2512 (2022).
69. Y. He, H. Wang, T. Hong, L. Hu, C. Gao, L. Gao, Y. Cui, R. Tan, D. Pu, J. Wu, HFM1 is essential for the germ cell intercellular bridge transport in primordial follicle formation in mice. *Cellular and molecular life sciences : CMLS* **82**, 28 (2024).
70. M. A. Garcia, L. Vardy, N. Koonrugsa, T. Toda, Fission yeast ch-TOG/XMAP215 homologue Alp14 connects mitotic spindles with the kinetochore and is a component of the Mad2-dependent spindle checkpoint. *The EMBO journal* **20**, 3389-3401 (2001).
71. A. J. Roberts, T. Kon, P. J. Knight, K. Sutoh, S. A. Burgess, Functions and mechanics of dynein motor proteins. *Nature reviews. Molecular cell biology* **14**, 713-726 (2013).
72. M. A. Cianfrocco, M. E. DeSantis, A. E. Leschziner, S. L. Reck-Peterson, Mechanism and regulation of cytoplasmic dynein. *Annual review of cell and developmental biology* **31**, 83-108 (2015).
73. S. L. Reck-Peterson, W. B. Redwine, R. D. Vale, A. P. Carter, The cytoplasmic dynein transport machinery and its many cargoes. *Nature reviews. Molecular cell biology* **19**, 382-398 (2018).
74. F. Gergely, V. M. Draviam, J. W. Raff, The ch-TOG/XMAP215 protein is essential for spindle pole organization in human somatic cells. *Genes & development* **17**, 336-341 (2003).
75. J. Q. Ni, R. Zhou, B. Czech, L. P. Liu, L. Holderbaum, D. Yang-Zhou, H. S. Shim, R. Tao, D. Handler, P. Karpowicz, R. Binari, M. Booker, J. Brennecke, L. A. Perkins, G. J. Hannon, N. Perrimon, A genome-scale shRNA resource for transgenic RNAi in Drosophila. *Nature methods* **8**, 405-407 (2011).
76. G. Minestrini, E. Mathe, D. M. Glover, Domains of the Pavarotti kinesin-like protein that direct its subcellular distribution: effects of mislocalisation on the tubulin and actin cytoskeleton during Drosophila oogenesis. *Journal of cell science* **115**, 725-736 (2002).

77. S. Nagarkar-Jaiswal, P. T. Lee, M. E. Campbell, K. Chen, S. Anguiano-Zarate, M. C. Gutierrez, T. Busby, W. W. Lin, Y. He, K. L. Schulze, B. W. Booth, M. Evans-Holm, K. J. Venken, R. W. Levis, A. C. Spradling, R. A. Hoskins, H. J. Bellen, A library of MiMICs allows tagging of genes and reversible, spatial and temporal knockdown of proteins in Drosophila. *eLife* **4**, (2015).
78. W. Lu, M. Winding, M. Lakonishok, J. Wildonger, V. I. Gelfand, Microtubule-microtubule sliding by kinesin-1 is essential for normal cytoplasmic streaming in Drosophila oocytes. *Proceedings of the National Academy of Sciences of the United States of America* **113**, E4995-5004 (2016).
79. V. Lantz, J. S. Chang, J. I. Horabin, D. Bopp, P. Schedl, The Drosophila orb RNA-binding protein is required for the formation of the egg chamber and establishment of polarity. *Genes & development* **8**, 598-613 (1994).
80. P. Rojas-Rios, A. Chartier, S. Pierson, D. Severac, C. Dantec, I. Busseau, M. Simonelig, Translational Control of Autophagy by Orb in the Drosophila Germline. *Developmental cell* **35**, 622-631 (2015).
81. W. Lu, M. Lakonishok, V. I. Gelfand, Kinesin-1-powered microtubule sliding initiates axonal regeneration in Drosophila cultured neurons. *Molecular biology of the cell* **26**, 1296-1307 (2015).
82. U. Del Castillo, M. Winding, W. Lu, V. I. Gelfand, Interplay between kinesin-1 and cortical dynein during axonal outgrowth and microtubule organization in Drosophila neurons. *eLife* **4**, (2015).
83. W. Lu, M. Lakonishok, R. Liu, N. Billington, A. Rich, M. Glotzer, J. R. Sellers, V. I. Gelfand, Competition between kinesin-1 and myosin-V defines Drosophila posterior determination. *eLife* **9**, (2020).
84. W. Lu, M. Lakonishok, A. S. Serpinskaya, D. Kirchenbuechler, S. C. Ling, V. I. Gelfand, Ooplasmic flow cooperates with transport and anchorage in Drosophila oocyte posterior determination. *The Journal of cell biology* **217**, 3497-3511 (2018).
85. L. K. Anderson, S. M. Royer, S. L. Page, K. S. McKim, A. Lai, M. A. Lilly, R. S. Hawley, Juxtaposition of C(2)M and the transverse filament protein C(3)G within the central region of Drosophila synaptonemal complex. *Proceedings of the National Academy of Sciences of the United States of America* **102**, 4482-4487 (2005).
86. M. Zaccai, H. D. Lipshitz, Differential distributions of two adducin-like protein isoforms in the Drosophila ovary and early embryo. *Zygote* **4**, 159-166 (1996).
87. C. H. Goldman, H. Neiswender, R. Veeranan-Karmegam, G. B. Gonsalvez, The Egalitarian binding partners Dynein light chain and Bicaudal-D act sequentially to link mRNA to the Dynein motor. *Development* **146**, (2019).

Acknowledgments

We thank many colleagues who generously shared reagents: Dr Daniel St Johnston (University of Cambridge), Dr Yukiko Yamashita (Whitehead Institute, MIT), Dr David Glover (Caltech), and the Bloomington *Drosophila* Stock Center (supported by NIH P40OD018537) for fly stocks; Dr Anna Akhmanova (Utrecht University) and the *Drosophila* Genomics Resource Center (DGRC, supported by NIH grant 2P40OD010949) for DNA constructs; Dr. Scott Hawley (Stowers Institute) for anti-C(3)G antibody. The anti-Orb4H8 monoclonal antibody deposited by the Paul D. Schedl group at Princeton University and the anti-Hts1B1 monoclonal antibody deposited by the Howard D. Lipshitz group at Hospital for Sick Children were obtained from the Developmental Studies Hybridoma Bank, created by the NICHD of the NIH and maintained at The University of Iowa, Department of Biology, Iowa City, IA 52242. We thank all current and past members of the Gelfand laboratory for their support, discussion, and suggestions, and the reviewers of this paper for their thoughtful comments.

Funding

This work was supported by the National Institute of General Medical Sciences (2R35GM131752 to V.I.G. and R35GM145340 to G.B.G.) and the CCBx Research Program of the Center for Computational Biology of the Flatiron Institute by the Simons Foundation to V.I.G. and W.L.

Author contributions

Conceptualization: WL, VIG

Methodology: WL, ML, HN, GBG, VIG

Investigation: WL, ML, HN, GBG, VIG

Formal analysis: WL, ML, HN, GBG, VIG

Data curation: WL, ML, HN, GBG, VIG

Visualization: WL, VIG

Supervision: GBG, VIG

Resources: GBG, VIG

Funding acquisition: WL, GBG, VIG

Project administration: GBG, VIG

Writing—original draft: WL, VIG

Writing—review & editing: WL, VIG

Competing Interests

All authors declare that they have no competing interests.

Data and Materials Availability

All data needed to evaluate the conclusions in the paper are present in the paper and the Supplementary Materials. All newly generated materials reported in this study, including *Drosophila* CRISPR knock-in lines, transgenic lines, and plasmids, are available from the corresponding authors upon request.

Table of contents for supplementary materials

Figs. S1 to S6

Movies S1 to S8

Figures and Figure Legends

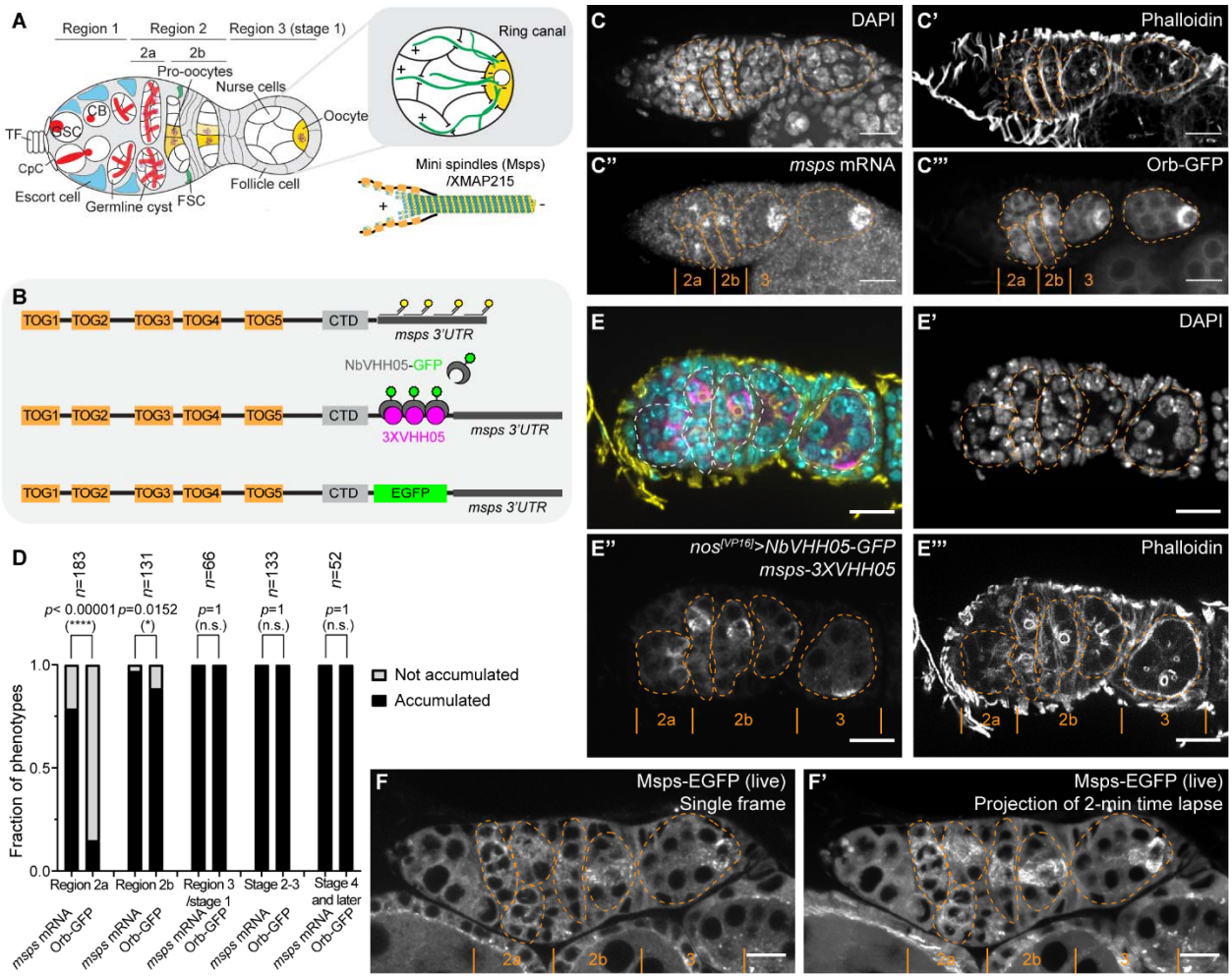

Fig. 1. Msps is concentrated in pro-oocytes and early oocytes.

(A) Left: schematic of a *Drosophila* germarium with spectrosome/fusome structures in red, meiotic synaptonemal complex in purple, and pro-oocytes/early oocytes in yellow. Inset: microtubule organization in early egg chambers, with most minus ends originating in the oocyte and plus ends extending through ring canals into nurse cells. Right: Mini spindles (Msps), the *Drosophila* homolog of XMAP215, promotes microtubule polymerization by delivering tubulin dimers to the plus-end via its five TOG domains.

(B) Domain organization of Msps/XMAP215 and methods used to visualize *msps* mRNA and protein localization. CTD, the C-terminal domain.

(C–C’’’) Representative *msps* mRNA localization in an Orb-GFP germarium. *msps* mRNA was detected by smiFISH against its 3′UTR (C’’).

(D) Quantification of *msps* mRNA and Orb-GFP accumulation across germarium regions and early egg chambers. Statistics between groups were performed using Fisher’s exact test.

(E–E’’’) Representative Msps protein localization in a fixed germarium. Msps-3XVHH05 was detected by germline-specific expression of a GFP-tagged nanobody against VHH05 (driven by *nos-Gal4*$^{[VP16]}$) (E’’).

(F–F’) Representative images of Msps-EGFP in a live germarium (single frame or 2-min time-lapse projection). See also movie S1.

(C–C’’’, E–F’) Orange dashed lines, germline cysts. Scale bars, 10 µm.

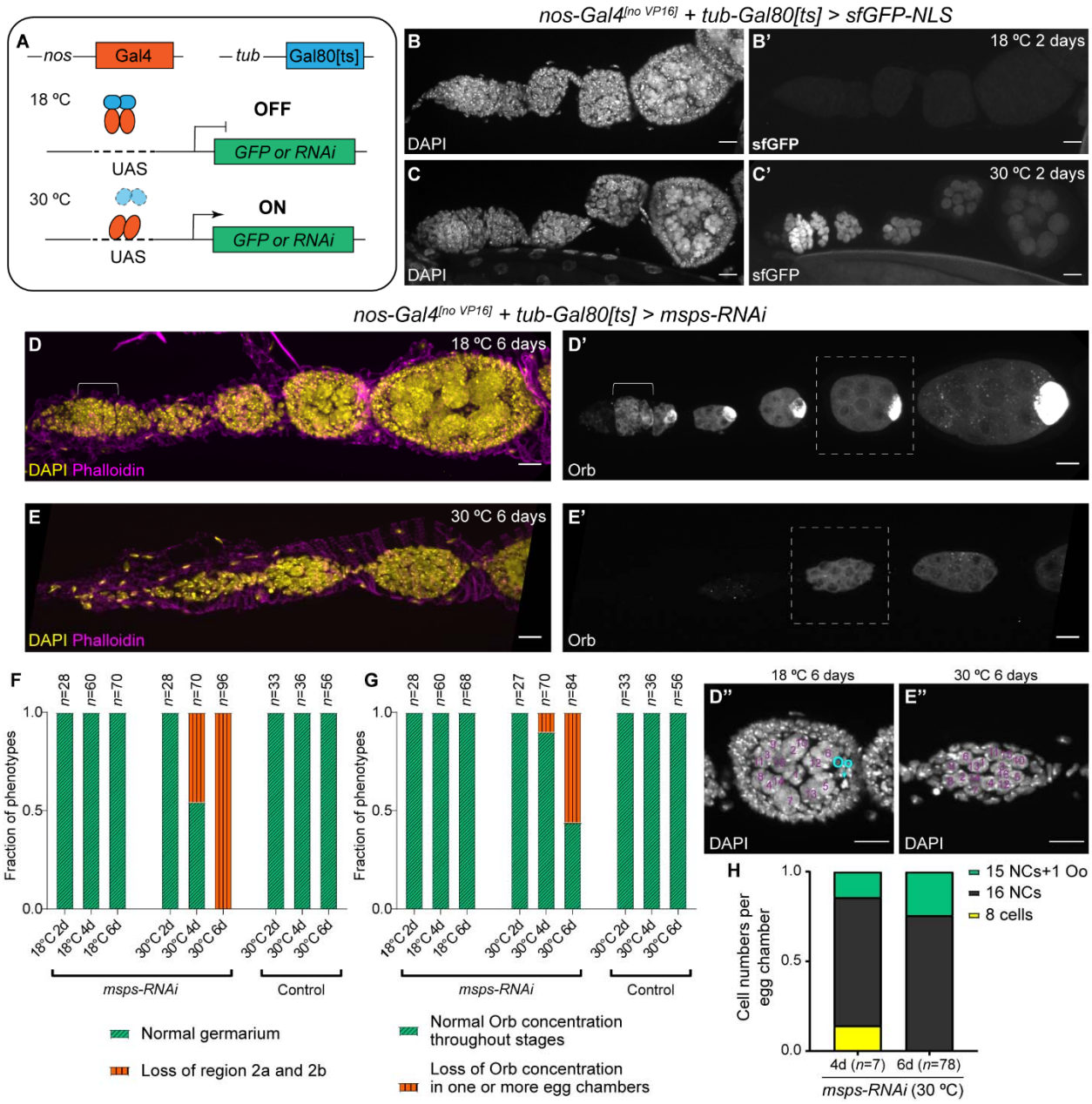

Fig. 2. Msps is required for oocyte specification.

(A) Schematic of the temperature-sensitive Gal80 system. At the permissive temperature (18 °C), Gal80[ts] binds Gal4 and prevents its interaction with upstream activating sequences (UAS), repressing transgene expression (OFF). At the restrictive temperature (30 °C), Gal80[ts] is inactivated, allowing Gal4 to activate UAS-driven transgenes (ON).

(B–C’) Germline expression of nuclear-localized superfolder GFP (sfGFP-NLS) using the Gal80[ts] system. Flies were raised at 18 °C, and F1 progeny were either maintained at 18 °C or shifted to 30 °C for 2 days before examination. Maximal z-projections of the GFP signal are shown in both cases.

(D–E’) Germline expression of *msps*-RNAi using the Gal80[ts] system. Flies were raised at 18 °C, and F1 progeny were either maintained at 18 °C or shifted to 30 °C for 6 days before examination. (D–D’) The white brackets indicate region 2a–2b of the germarium. (D’’–E’’) DAPI staining of the regions outlined by white dashed boxes in (D’–E’). Nurse cell nuclei are numbered in purple, and the oocyte nucleus is indicated in cyan. See also movies S2 and S3.

(F–G) Quantifications of germaria lacking region 2a/2b and of ovarioles lacking Orb concentration in the listed genotypes. All crosses were raised at 18 °C; F1 progeny were maintained at 18 °C or shifted to 30 °C for the indicated number of days. Sibling flies carrying *tub-Gal80[ts]* but lacking *msps*-RNAi served as controls.

(H) Summary of cell numbers in egg chambers lacking Orb concentration.

(B–E’’) Scale bars, 10 µm.

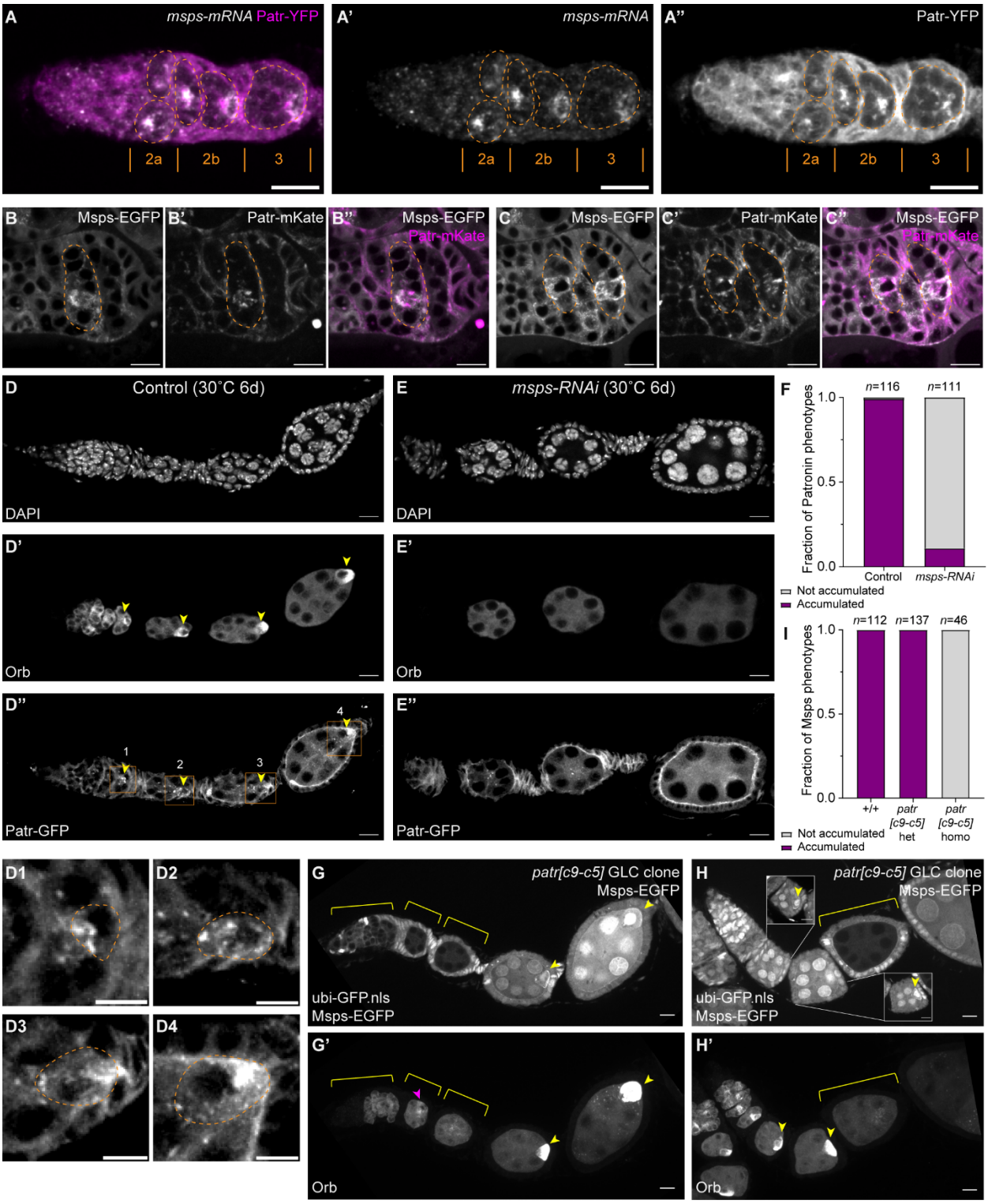

Fig. 3. Msps and Patronin are interdependent for oocyte specification and localization.

(A–A’’) Localization of *msps* mRNA (smiFISH) and YFP-tagged Patronin protein. Orange dashed lines, germline cysts.

(B–C’’) Localization of EGFP-tagged Msps and mKate-tagged Patronin. Maximal projection of 2-min time-lapse images at two focal planes of the same germarium. Orange dashed lines, germline cysts. See also movie S4.

(D–E’’) Orb staining (D’–E’) and Patronin localization (*ubi-Patronin-GFP*, D’’–E’’) in control (D–D’’) and *msps*-RNAi (E–E’’) samples. Flies were raised at 18 °C and shifted to 30 °C for 6 days. Accumulation of Orb and Patronin in the oocyte (yellow arrowheads, D’–D’’; D1-D4, zoom-in areas of the regions indicated by the orange boxes in D’’, with oocytes outlined by orange dashed lines) was abolished in *msps*-RNAi (E’–E’’). Sibling flies carrying *ubi-Patronin-GFP* and *tub-Gal80[ts]*, but lacking *msps-RNAi*, were used as controls.

(F) Quantification of Patronin localization phenotypes in control and *msps*-RNAi samples.

(G–H’) Msps-EGFP (G–H) and Orb staining (G–H’) in *patr[c9-c5]* FRT clones. *patr[c9-c5]* homozygous clones (yellow brackets) lack nuclear GFP; heterozygous cells retain nuclear GFP. Yellow arrowheads mark Msps-EGFP and Orb accumulation in *patr[c9-c5]* heterozygous oocytes. Insets in (H) show Msps-EGFP accumulation in the oocytes at different focal planes. Magenta arrowhead in (G’) highlights residual Orb signal in *patr[c9-c5]* homozygous clones.

(I) Quantification of Msps localization phenotypes in control clones (FRT G13), *patr[c9-c5]* heterozygotes, and *patr[c9-c5]* homozygous clones.

1113 (A–E'', G–H') Scale bars, 10 µm. (D1-D4) Scale bars, 5 µm.

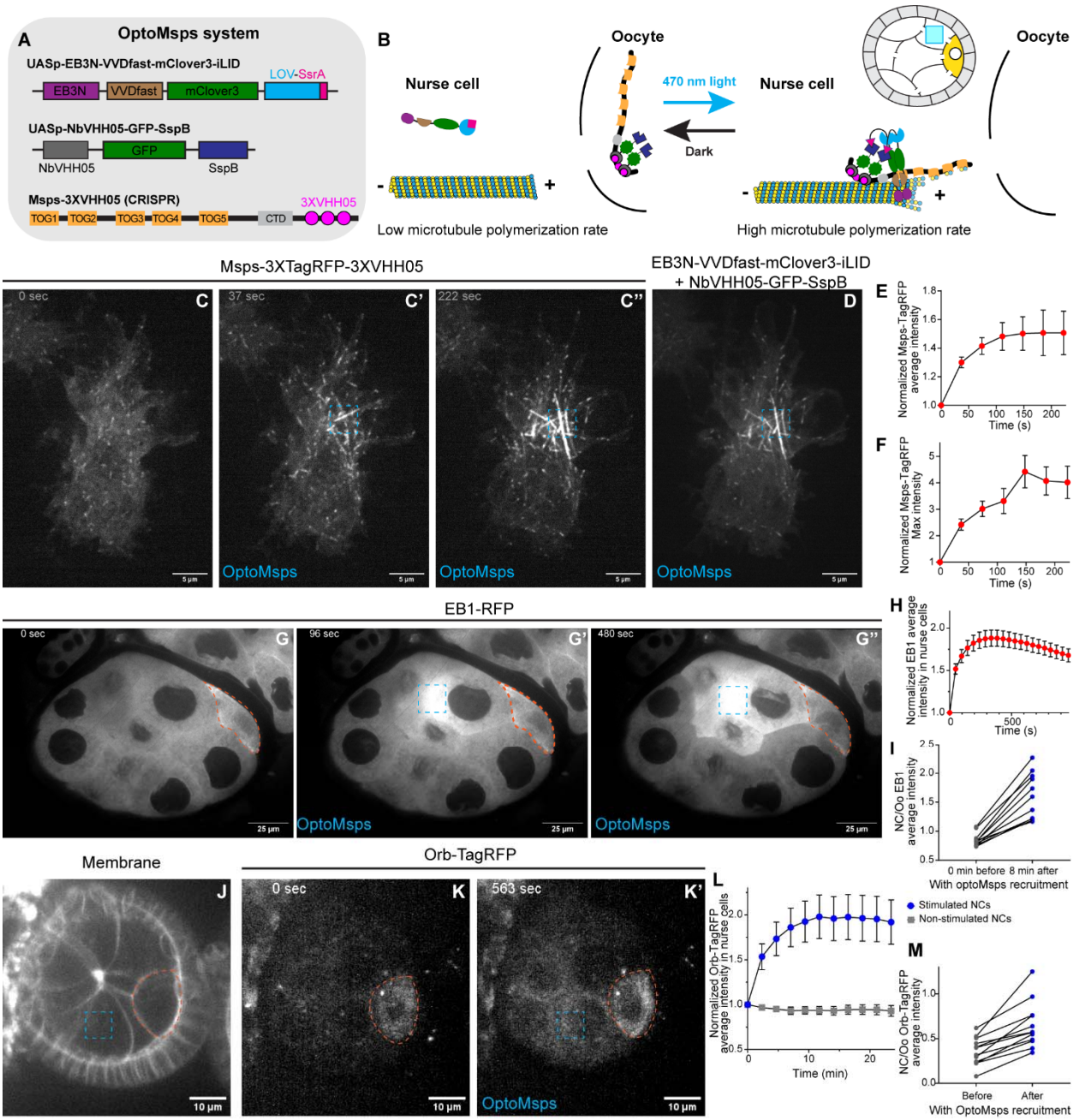

Fig. 4. Msps is sufficient to initiate oocyte specification.

(A) Schematic of the OptoMsps system, composed of three elements: (1) EB3N fused to the blue light–sensitive dimerization module VVDfast, followed by LOV2-SsrA; (2) SspB fused to a nanobody recognizing the VHH05 NanoTag; and (3) a CRISPR knock-in of three copies of the VHH05 NanoTag into endogenous *msps*.

(B) Cartoon illustrating OptoMsps recruitment: blue light induces VVDfast homodimerization and LOV2-SsrA/SspB heterodimerization, driving recruitment of Msps to microtubules.

(C–F) Validation of OptoMsps in S2R+ cells. (C–C'') Msps-3XTagRFP-3XVHH05 before and after local blue-light illumination (blue dashed box). (D) End-point GFP channel showing localization of the OptoMsps components. (E–F) Quantifications (mean ± SEM, *n*=7) of normalized average and maximum TagRFP intensity in the illuminated region. See also movie S5.

(G–I) OptoMsps increases EB1 signal in nurse cells. (G–G'') EB1-RFP before and after local blue-light illumination in nurse cells (blue dashed box). Orange dashed outline, oocyte. (H) Quantification (mean ± SEM, *n*=12) of normalized average EB1-RFP intensity in illuminated nurse cells. (I) Ratio of EB1-RFP intensity in illuminated nurse cells to that in the oocyte (NC/Oo) before and 8 min after illumination (*n*=11). See also movie S7.

(J–M) OptoMsps increases Orb intensity in nurse cells. (J) Membrane outline of the egg chamber, with the oocyte (orange dashed line) and the blue-light illumination region (blue dashed box). (K–K') Orb-TagRFP before and after local Msps recruitment in nurse cells. (L) Quantification (mean ± SEM) of normalized average Orb-TagRFP intensity across entire nurse cells in blue-light–illuminated egg chambers (blue dots, *n*=12) versus non-illuminated nurse cells in neighboring egg chambers (gray squares, *n*=13). (M) Ratio of Orb-TagRFP intensity in entire nurse cells to that in the oocyte (NC/Oo) before and after illumination (*n*=12). See also movie S8.

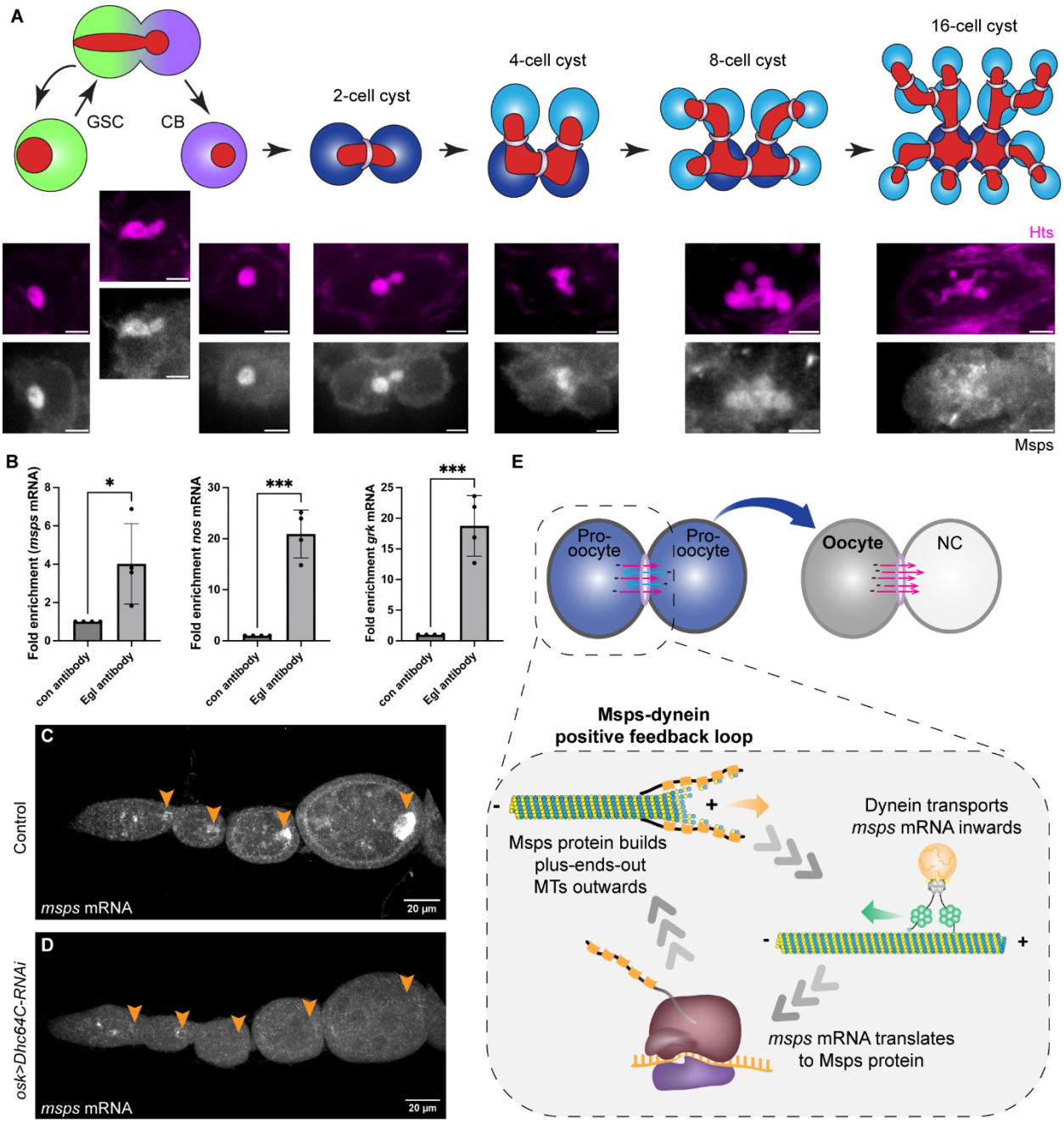

Fig. 5. Msps initiates a positive feedback loop for oocyte specification.

(A) Msps association with the spectrosome and fusome structures in successive germline stages: germline stem cells (GSCs), cystoblasts (CBs), 2-cell, 4-cell, and 8-cell cysts. In 16-cell cysts, Msps shows a more diffuse “cloudy” distribution around the branched fusome. Msps was endogenously tagged with 3XVHH05 and visualized using

a germline-expressed VHH05-specific nanobody, NbVHH05-3XTagRFP (*nos-Gal4*$^{[VP16]}$). Scale bars, 2 µm.

(B) Interaction of Egalitarian (Egl) with *msps* mRNA compared to two known Egl-dependent cargos, *nanos* (*nos*) and *gurken* (*grk*).

(C-D) *msps* mRNA distribution in control (*osk-Gal4*$^{[VP16]}$/+) and *Dhc64C-RNAi* (*UAS-Dhc64C-RNAi/+; osk-Gal4*$^{[VP16]}$/+) ovarioles. Oocytes are marked by orange arrowheads.

(E) A positive feedback mechanism amplifies a small difference in Msps protein distribution and microtubule polarity between the two pro-oocytes into a definitive oocyte fate decision.